

Journal Pre-proofs

Copper(II) hydrazone complexes with different nuclearities and geometries: Synthesis, structural characterization, antioxidant SOD activity and antiproliferative properties

A.K. Patel, R.N. Jadeja, H. Roy, R.N. Patel, S.K. Patel, R.J. Butcher, M. Cortijo, S. Herrero

PII: S0277-5387(20)30281-3
DOI: <https://doi.org/10.1016/j.poly.2020.114624>
Reference: POLY 114624

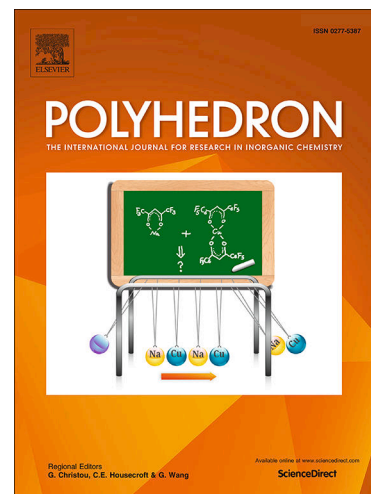
To appear in: *Polyhedron*

Received Date: 20 April 2020
Revised Date: 17 May 2020
Accepted Date: 19 May 2020

Please cite this article as: A.K. Patel, R.N. Jadeja, H. Roy, R.N. Patel, S.K. Patel, R.J. Butcher, M. Cortijo, S. Herrero, Copper(II) hydrazone complexes with different nuclearities and geometries: Synthesis, structural characterization, antioxidant SOD activity and antiproliferative properties, *Polyhedron* (2020), doi: <https://doi.org/10.1016/j.poly.2020.114624>

This is a PDF file of an article that has undergone enhancements after acceptance, such as the addition of a cover page and metadata, and formatting for readability, but it is not yet the definitive version of record. This version will undergo additional copyediting, typesetting and review before it is published in its final form, but we are providing this version to give early visibility of the article. Please note that, during the production process, errors may be discovered which could affect the content, and all legal disclaimers that apply to the journal pertain.

© 2020 Published by Elsevier Ltd.



Copper(II) hydrazone complexes with different nuclearities and geometries: Synthesis, structural characterization, antioxidant SOD activity and antiproliferative properties

A.K. Patel^a, R.N. Jadeja^a, H. Roy^b, R.N. Patel^c, S.K. Patel^c, R.J. Butcher^d, M. Cortijo^e, S. Herrero^e.

^aDepartment of Chemistry, Faculty of Science, The Maharaja Sayajirao University of Baroda, Vadodara 390002, India.

^bDepartment of Zoology, Faculty of Science, The Maharaja Sayajirao University of Baroda, Vadodara 390002, India.

^cDepartment of Chemistry, A.P.S. University, Rewa, M.P 486003, India.

^dDepartment of Inorganic & Structural Chemistry, Howard University, Washington, DC 22031, USA.

^eDepartamento de Química Inorgánica, Facultad de Ciencias Químicas, Universidad Complutense, 28040, Madrid, Spain.

Abstract

New copper(II) hydrazone complexes with (Z)-2-(phenyl(2-(pyridin-2-yl)hydrazono)methyl)pyridine (L) were synthesized and characterized using various physicochemical methods. The geometries of the complexes can be classified as mononuclear and binuclear. The complex **1**, [Cu(L)Cl₂], is mononuclear whereas the solid-state structure of complex **2** contain a mixture of co-crystals of the mono- and binuclear complexes **2a**, [Cu(L)(H₂O)(SO₄)], and **2b**, [(L)Cu-(SO₄)₂-Cu(L)]. The molecular structure of **2** contains two units of the mononuclear complex **2a** and two units of the binuclear complex **2b**. The copper atoms contained in all the mono- and binuclear complexes are in a distorted square pyramidal geometry. The present study indicates that complexes having different nuclearities and geometries can be achieved by changing the synthetic conditions and methods. Variable temperature magnetic susceptibility measurements of the complexes have shown the presence of weak anti-ferromagnetic interactions. These interactions are mediated by intermolecular hydrogen bonding in **1** and through a symmetric sulfate bridge in **2**. The EPR spectra in the polycrystalline state for **1** and **2** exhibited a broad signal at ~2.149 due to spin-spin interactions between two copper(II) ions. The cyclic voltammograms of complexes **1** and **2** in DMSO gave two irreversible redox waves. Density functional theory (DFT) calculations were evaluated in the study, involving the molecular specification with the use of B3LYP/LANL2DZ formalism for the copper atoms and B3LYP/6-31G for the remaining atoms. Both complexes catalyzed the dismutation of superoxide (O₂⁻). Furthermore, the copper complexes and the ligand were tested to explore their anticancer properties. Promising cytotoxicity of the synthesized compounds was observed against the selected cancerous cell lines of neuroblastoma, lung carcinoma, hepatocellular carcinoma and breast cancer.

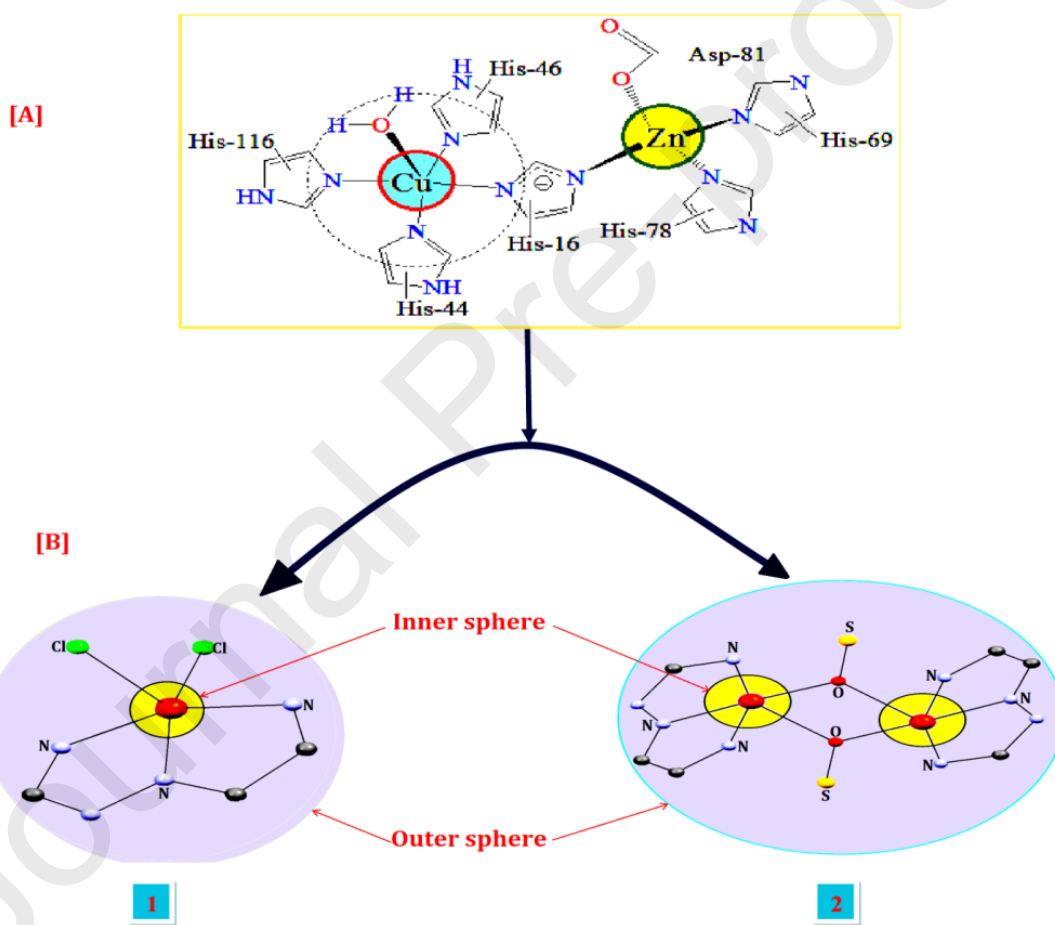
Keywords: Copper(II) complexes, electron paramagnetic resonance (Epr), magnetic measurements, cyclic voltammograms, biological studies.

1. Introduction

The chemistry of hydrazones and their transition metal complexes is an interesting area of research due to their wide variety of chemical structures with different physicochemical properties¹⁻⁴. They have potential applications in molecular recognition, catalysis and nanomaterials due to their mild reaction conditions and high synthetic rates for Schiff base complexes⁵⁻⁸. Additionally, copper and Schiff base complexes have potential biological applications owing to their stability and biocompatibility⁹. Copper(II) Schiff base complexes have been receiving considerable attention. The flexibility of the coordination sphere around the copper(II) ion along with other atoms leads to structural diversity¹⁰⁻¹⁴. Copper(II) complexes provide models for metalloprotein activities and insight towards the design of new catalysts. Hydrazone Schiff bases are organic compounds with suitable structural features and can form metal chelates either as a neutral ligand (HL) or in the mono-anionic form (L⁻). The coordination possibilities of hydrazones are introduced by using different substituted aldehydes or ketones, which includes additional donor atoms¹⁵⁻²⁰. Coordination complexes containing such ligands with transition metals yield monometallic, bis-chelated, bi- and multi-metallic complexes²¹. Hydrazones also have continued attention due to their structural diversity and coordination properties. Recently, the design and application of low molecular weight copper complexes as superoxide dismutase mimics have received great attention. Several copper(II) complexes have been designed and characterized as potent models of enzymes, including Schiff base complexes²².

The present paper is devoted to structural, magneto-chemical and quantum chemical (DFT) calculations using the (Z)-2-(phenyl(2-(pyridin-2-yl)hydrazone)methyl)pyridine ligand. The extent of the deprotonation depends on the reaction conditions and the metal^{23,24}. The hydrazone Schiff base inspired us to investigate the nature of the coordination as well as the structural properties of copper(II) complexes with (Z)-2-(phenyl(2-(pyridin-2-yl)hydrazone)methyl)pyridine (HL), viz. [Cu(Cl)₂(L)] (**1**) and [Cu₂(μ-SO₄)₂(L)₂] (**2**). The molecular structures of these complexes were determined using single-crystal X-ray analysis. Both complexes were further character using other physicochemical techniques (UV-vis, IR, CV and DPV). These two complexes were also studied using electron paramagnetic resonance (EPR) spectroscopy. This technique is widely used for the

characterization of paramagnetic species²⁵⁻²⁷. The technique enables important insight into the description of the chemical environment and binding pattern around the metal center. These complexes have the catalyzing copper(II) N_3Cl_2/N_3O_2 structural motifs as their inner sphere structure (Scheme 1). The coordination sites available for the binding of O_2^- are shown by single-crystal X-ray structures. Additionally, the antioxidant superoxide dismutase activity data for both complexes were collected and compared with reported SOD models. The anticancer activities of the compounds toward human IMR 32 (neuroblastoma), MCF 7 (breast cancer), HepG2 (hepatocellular carcinoma) and A549 (lung cells) cancer cell lines have been examined and compared against cisplatin under identical conditions using an MTT assay.



Scheme 1. Synthesis of complexes **1** and **2** based on the active site structure of Cu-Zn SOD. [A] The structure of Cu-Zn SOD. [B] Structures of complexes **1** and **2**.

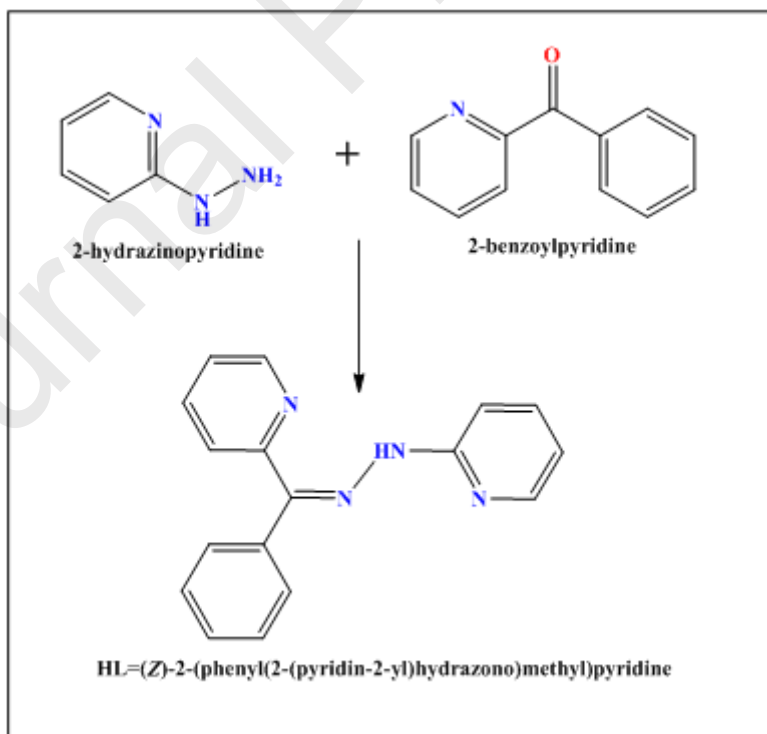
2. Experimental

2.1. Materials and instrumentation

All solvents were dried and distilled before use following standard procedures²⁸. Reagent grade chemicals were used throughout and HPLC grade solvents were employed for spectroscopic studies. The metal salts were purchased from Sigma-Aldrich Chemical Co. Pvt. Ltd. and used as received.

2.2. Synthesis of the ligand (HL)

The Schiff base ligand HL = (Z)-2-(phenyl(2-(pyridin-2-yl)hydrazono)methyl)pyridine was synthesized by taking 2-hydrazinopyridine (1.091 g, 10 mmol) in absolute ethanol (50 ml) and then 2-benzoylpyridine (0.78 g, 10 mmol) was added with a few drops of glacial acetic acid as a catalyst. The synthesis of the ligand is shown in Scheme 2. The resultant mixture was stirred at room temperature for 30 min and then refluxed at 75 °C for 3 h. The yellowish solution was filtered and the filtrate was kept for slow evaporation at room temperature to yield a light yellow polycrystalline sample. The Schiff base was washed with ethanol and dried over fused CaCl₂. Yield 1.10g (75%). Anal. Calc. for C₁₇H₁₄N₄ (274.33): C, 74.52; H, 5.54; N, 20.04 %. Found: C, 74.43; H, 5.14; N, 20.42 %. FT-IR (KBr, cm⁻¹): 1592 ν (C=N). ¹H NMR (CDCl₃) δ , ppm: 8.00-7.29 (s, 3H, CH benzylidenimine), 8.861–7.89 (s, 8H, CH 2-pyridine), and 13.0 (s, 1H, NH hydrazide). The ¹H-NMR spectrum is presented in (Fig. S1).



Scheme 2. Synthetic route to the ligand HL.

2.3. Synthesis of the complex [Cu(Cl)₂(L)] (1)

The Schiff base ligand (0.274 g, 1.0 mmol) was dissolved in methanol (20 mL). A solution of CuCl₂·2H₂O (0.134 g, 1.0 mmol) in methanol (20 mL) was added dropwise to the above solution, followed by stirring for 5 h to give a green clear solution. The resulting solution was filtered. The filtrate was left for slow evaporation at room temperature. Plate-like crystals were formed from the solution two weeks later. These crystals were washed with hot distilled water and then ethanol to remove impurities. The crystals were dried under vacuum. Yield 0.380 g (80%). Anal. Calc. for C₁₇H₁₅Cl₂CuN₄ (408.77): C, 49.80; H, 3.65; N, 13.61 %. Found: C, 49.83; H, 3.69; N, 13.67 %. FT-IR (KBr, cm⁻¹): 1564 ν(C=N), 417 (s) ν(Cu-N).

2.4. Synthesis of the complex [Cu₂(μ-SO₄)₂(L)₂] (2)

The Schiff base ligand (0.274 g, 1.0 mmol) was dissolved in methanol (20 mL). A solution of CuSO₄·5H₂O (0.159 g, 1.0 mmol) in methanol (20 mL) was added dropwise to the above solution, followed by stirring for 5 h to give a green clear solution. The resulting solution was filtered. The filtrate was left for slow evaporation at room temperature. Plate-like crystals were formed from the solution two weeks later. These crystals were washed with hot distilled water and then ethanol to remove impurities. The crystals were dried under vacuum. Yield 0.380 g (80%). Anal. Calc. for C₆₈H₈₀Cu₄N₁₆O₂₈S₄ (1951.88): C, 46.82; H, 3.75; N, 12.35 %. Found: C, 46.95; H, 3.48; N, 12.88 %. FT-IR (KBr, cm⁻¹): 1568 ν(C=N), 462 (s) ν(Cu-O), 417 (s) ν(Cu-N).

2.5. Methods and physical measurements

Elemental analyses were carried out using an Elementar Vario EL III Carlo Erba 1108 Analyzer. The ¹H NMR spectrum of the ligand was recorded in CDCl₃ on a Bruker Advance 400 (FT-NMR) multinuclear spectrometer. Chemical shifts are reported in parts per million (ppm) using tetramethylsilane (TMS) as an internal standard. The accelerating voltage was 10 kV and the spectra were recorded at room temperature. UV-vis spectra were recorded at room temperature using a Shimadzu UV-vis spectrophotometer UV-1601 in quartz cells. Infrared (IR) spectra (4000-400 cm⁻¹) were collected using the KBr pellet technique on a Perkin-Elmer spectrophotometer. The low and room temperature electron paramagnetic resonance (EPR) spectra were recorded using a Varian E-line Century Series spectrometer equipped with a dual cavity and operating at the X-band with 100 kHz modulation frequency. Varian quartz tubes were used for measuring EPR spectra of

polycrystalline samples and frozen solutions. The EPR spectra were calibrated with tetracyanoethylene (TCNE) as a marker ($g = 2.00277$). The EPR parameters for the copper(II) complexes were determined accurately from the computer simulation program¹⁹. The mass spectrum of the ligand was recorded on a Trace GC ultra DSQ II. Cyclic voltammetry was performed using a BAS-100 Epsilon Electrochemical Analyzer on the complexes in DMSO solutions using Ag/AgCl and glassy carbon as reference electrodes. All measurements were carried out at room temperature under a nitrogen atmosphere. The concentrations of the solutions were 10^{-3} mol dm⁻³ with respect to the complexes and 0.1 mol dm⁻³ with respect to tetrabutylammonium perchlorate (TBAP) as a supporting electrolyte. Ferrocene (Fe) was added to the solution as an internal standard. Magnetic measurements at variable temperatures were performed on crushed single crystals of the complexes using a Quantum Design MPMSXL SQUID (Superconducting Quantum Interference Device) magnetometer. The measurements were performed over the temperature range 2-300 K under a magnetic field of 0.5 T. The data were corrected for the intrinsic diamagnetic contributions based on Pascal's constants, the Temperature-Independent Paramagnetism (TIP) and the sample holder contribution. X-ray crystallographic data of the complexes were collected on a Bruker APEX-II diffractometer using graphite monochromated MoK α radiation ($\lambda = 0.71073$ Å). The crystal orientation, cell refinement and intensity measurements were made using CAD-4PC performing C-scan measurements. The structures were solved by direct methods using SHELXS-97 and refined by full-matrix least-squares using SHELXL-97²⁹⁻³². Crystallographic data of the complexes were collected on a Rigaku-Oxford Diffraction Gemini Eos diffractometer using graphite monochromated CuK α radiation ($\lambda = 1.54184$ Å) for L and graphite monochromated MoK α radiation for **1** and **2**, respectively. For both systems, all non-hydrogen atoms were refined anisotropically and all hydrogen atoms were geometrically fixed in calculated positions. Crystals suitable for single-crystal X-ray analysis of both complexes were grown by slow evaporation of the reaction mixtures at room temperature. Single crystals of suitable dimensions for single-crystal X-ray analysis were mounted on glass fibers for the Bruker instrument and polymer loops for the Gemini instrument and used for data collection. A simultaneous TGA was performed using a TG-DTA 6300 INCARP EXSTAR 6000 at a heating rate of 10 °C/min in the temperature range 25-600 °C with a nitrogen atmosphere maintained throughout the measurement.

2.6. Computational study

Theoretical calculations by density functional theory (DFT) were performed with regard to molecular structure optimization and HOMO-LUMO energies etc. of complexes **1** and **2**. Full geometry optimizations were carried out using the density functional theory (DFT) method at the B3LYP level for the complexes³³. All DFT calculations were carried out starting from the experimental single-crystal X-ray data for the input geometries. All elements except Cu were assigned the LANL2DZ basis set³⁴. LANL2DZ with an effective core potential was used for the Cu atom³⁵. In the computational model, the cationic complex was taken into account. All calculations were carried out with the GAUSSIAN09 program,³⁶ with the aid of the Gauss View visualization program. Vertical electronic excitations based on B3LYP optimized geometries were evaluated using the time-dependent density functional theory (TDDFT) formalism³⁷ in DMSO, using a conductor-like polarizable continuum model (CPCM)³⁸.

2.7. Antioxidant SOD activity

The antioxidant SOD activities of complexes **1** and **2** were assessed using alkaline DMSO as a source of superoxide radical ($O_2^{\cdot-}$) and nitro blue tetrazolium chloride (NBT) as a scavenger³⁹⁻⁴¹. The quantitative reduction of NBT to formazan by $O_2^{\cdot-}$ was followed spectrophotometrically at 450 nm. The SOD activity was obtained by plotting the percentage inhibition of NBT reduction (%) vs the concentrations of the complexes. The unit of SOD activity is the concentration of the enzyme or complex that induces a 50% inhibition (IC_{50}) in the reduction of NBT. Two assays were carried out for each concentration of the metal complex.

2.8. Anti-cancer activity

The antiproliferative properties of the present complexes were studied *in vitro* on various carcinoma cell lines.

2.8.1. Cell culture conditions

For the cytotoxicity determination, we used four different human cancer cell lines, viz. IMR 32 (neuroblastoma), MCF 7 (breast cancer), HepG2 (hepatocellular carcinoma) and A549 (lung cells), which were procured from the National Center for Cell Science (NCCS), Pune. Cells were cultured in Dulbecco's Modified Eagle Medium (DMEM) supplemented with 10% FBS and 1% antibiotics. All the cell lines were maintained at a temperature of 37 °C with 100% relative humidity and 5% CO_2 .

2.8.2. Cytotoxicity assay

Cell viability was measured using an MTT assay (MTT = 3-(4,5-dimethyl-2-thiazolyl)-2,5-diphenyl-2H-tetrazolium bromide). Cells were seeded in 96 well plates at a density of 8000 cells/well and incubated overnight for cell adhesion. Cells were treated with the synthesized compound for 24 h and incubated at 37 °C temperature in a CO₂ incubator. Cisplatin was used as a reference drug. After the incubation time, the cells were washed with PBS and exposed to MTT (5 mg/ml) for 4 h in the dark at 37 °C. The medium with MTT was removed and formed formazan crystal was dissolved in 200 ml of DMSO. At the end of the reaction, the optical density was measured at 540 nm using an ELISA plate reader (ELX800 Universal Microplate Reader, USA). The % inhibition concentration was calculated using the formula: % inhibition concentration = 100 - (OD of treated/OD of Control) × 100.

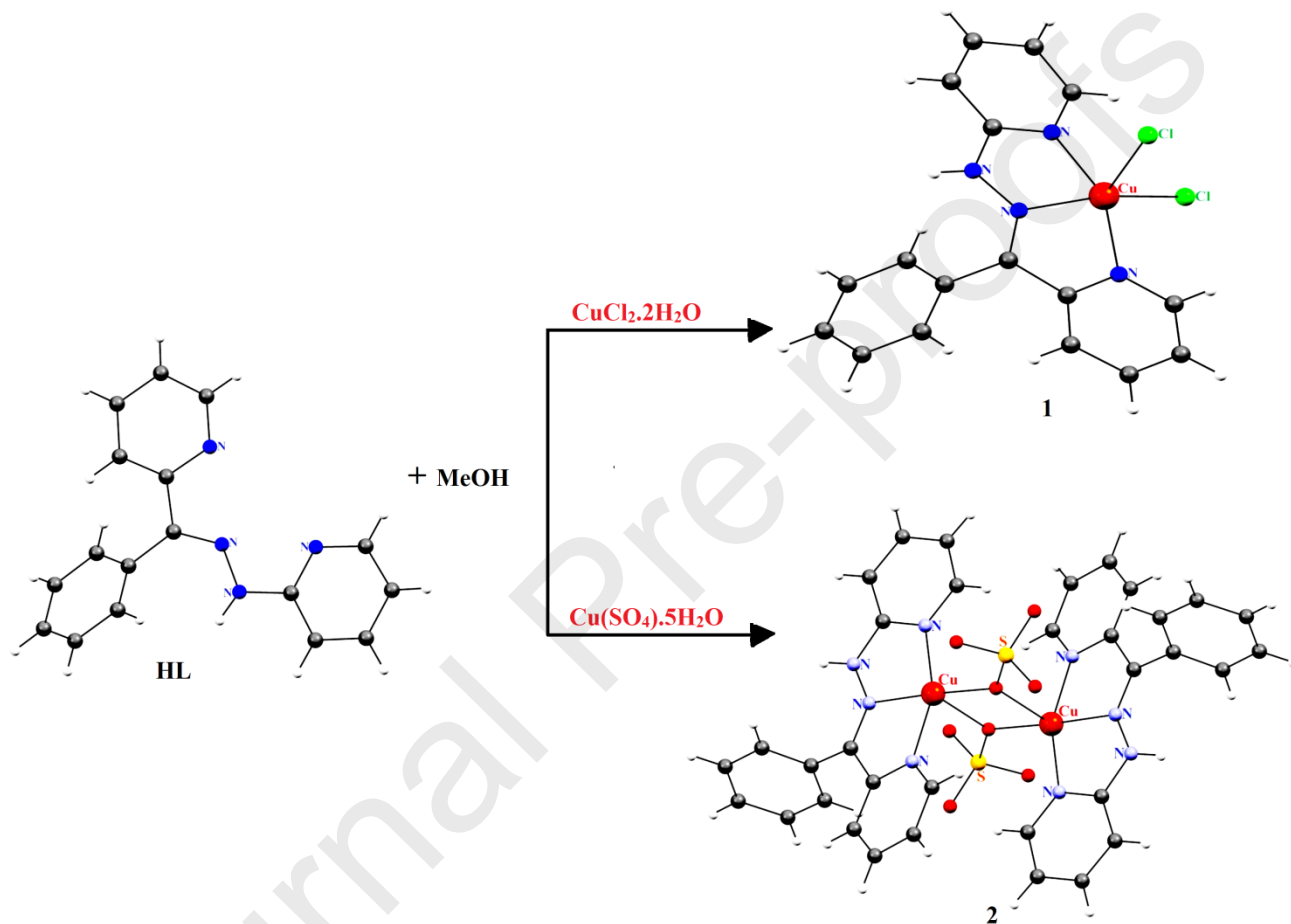
3. Results and discussion

The copper(II) complexes, having the general composition [Cu(Cl)₂(L)] **1** and [Cu₂(μ-SO₄)₂(L)₂] **2**, were synthesized by a general procedure. These complexes have been characterized by FT-IR, UV-Vis, CV and X-ray analysis. The SOD and anti-cancer activities of the complexes have also been evaluated. The complexes are insoluble in water and non-polar solvents, but are soluble in MeOH, EtOH, DMF, DMSO, acetonitrile and chlorinated solvents.

3.1. Synthesis and structural characterization

The reaction of the Schiff base (HL) from the condensation of 2-hydroxy-1-naphthaldehyde and acethydrazide with either CuCl₂.2H₂O and Cu(SO₄).5H₂O in a 1:1 molar ratio yields [Cu(Cl)₂(L)] **1** and [Cu₂(μ-SO₄)₂(L)₂] **2**, in which the NH group of HL remains deprotonated. The synthetic routes used for the synthesis of **1** and **2** are depicted in Scheme 3. These complexes were synthesized in good yield. Both complexes **1** and **2** are air-stable. All general characterizations were carried out with crystalline samples. Microanalyses showed that the components of both complexes are consistent with the results of the molecular structural analysis. Single crystal X-ray analysis showed that complex **1** is mononuclear, whereas **2** is a binuclear complex. In the IR spectrum of complex **1**, the peaks at 3433 and 1459 cm⁻¹ are characteristic for N-H stretching and bending modes respectively. Similarly for complex **2**, peaks at 3406 and 1464 cm⁻¹ are observed. The sharp >C=N stretching vibration bands, corresponding to the imine group of Schiff base framework, appear at 1568 cm⁻¹ and the skeleton vibrations of the phenyl groups are at 1480 and 1542 cm⁻¹. The redshifts in

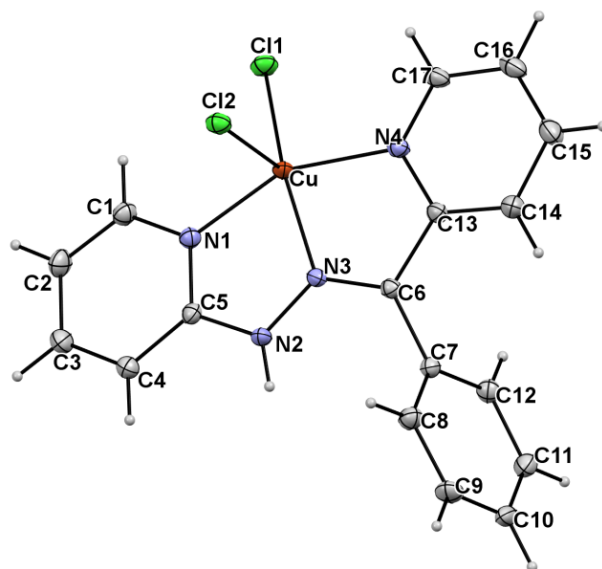
the vibrational absorption bands of the $>C=N$ group, compared to 1592 cm^{-1} for the free Schiff base, are in agreement with the coordination of the Schiff base to the copper(II) center⁴². The observed vibrational bands at 427 and 462 cm^{-1} are due to $\nu(M-N)$ and $\nu(M-O)$ stretching frequencies in complex **2**. Other bands associated with the Schiff base showed minor shifts, suggesting that the electron density of the bonds have been altered on coordination⁴³. The FT-IR spectra are given in Figs. S2-S4.



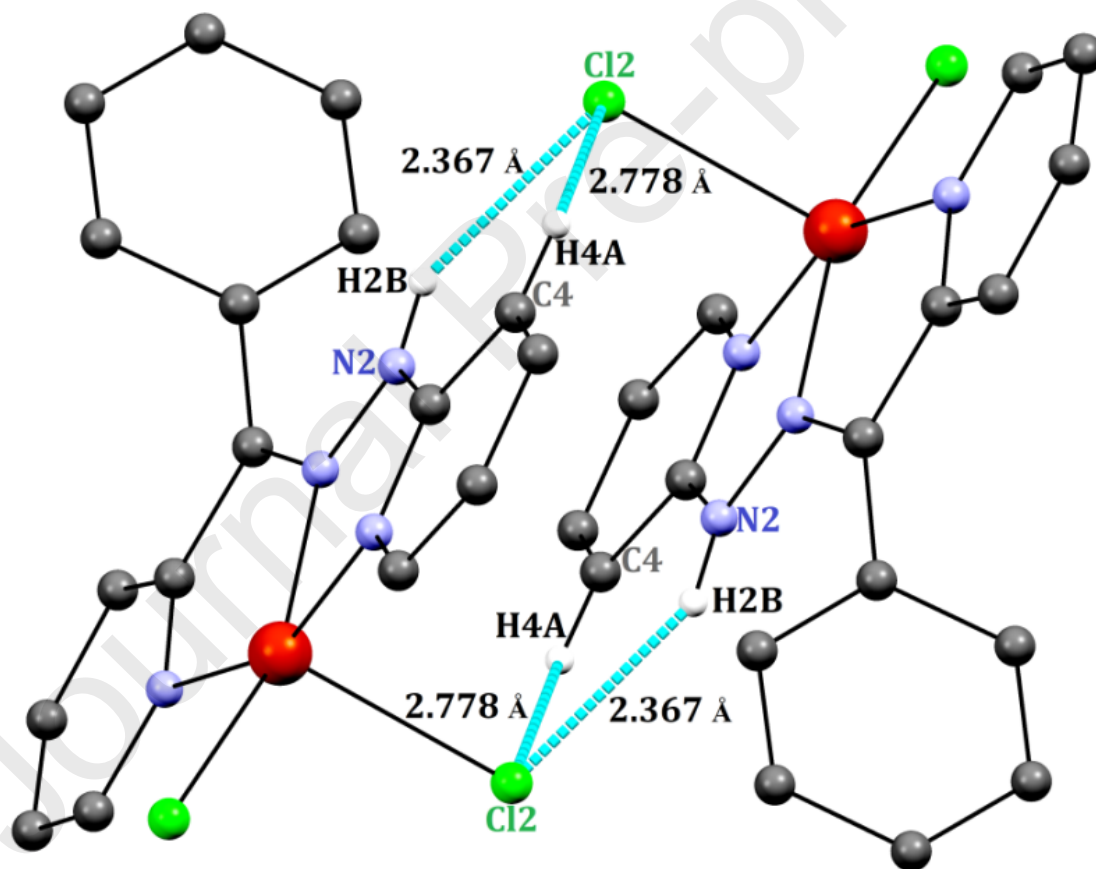
Scheme 3. Synthetic routes to the metal complexes **1** and **2**.

3.2. Molecular structure characterization

The molecular structures of both complexes are shown in Figs. 1 and 2 respectively. Complex **1** is mononuclear, whereas **2** is a binuclear complex. The crystal data and structure refinement details are shown in Table 1. Selected bond distances and angles are presented in Table 2. In both complexes, the Schiff base ligand acts tridentate *via* the NNN donor atom set and it is mono diprotonated (L^-).



(a)



(b)

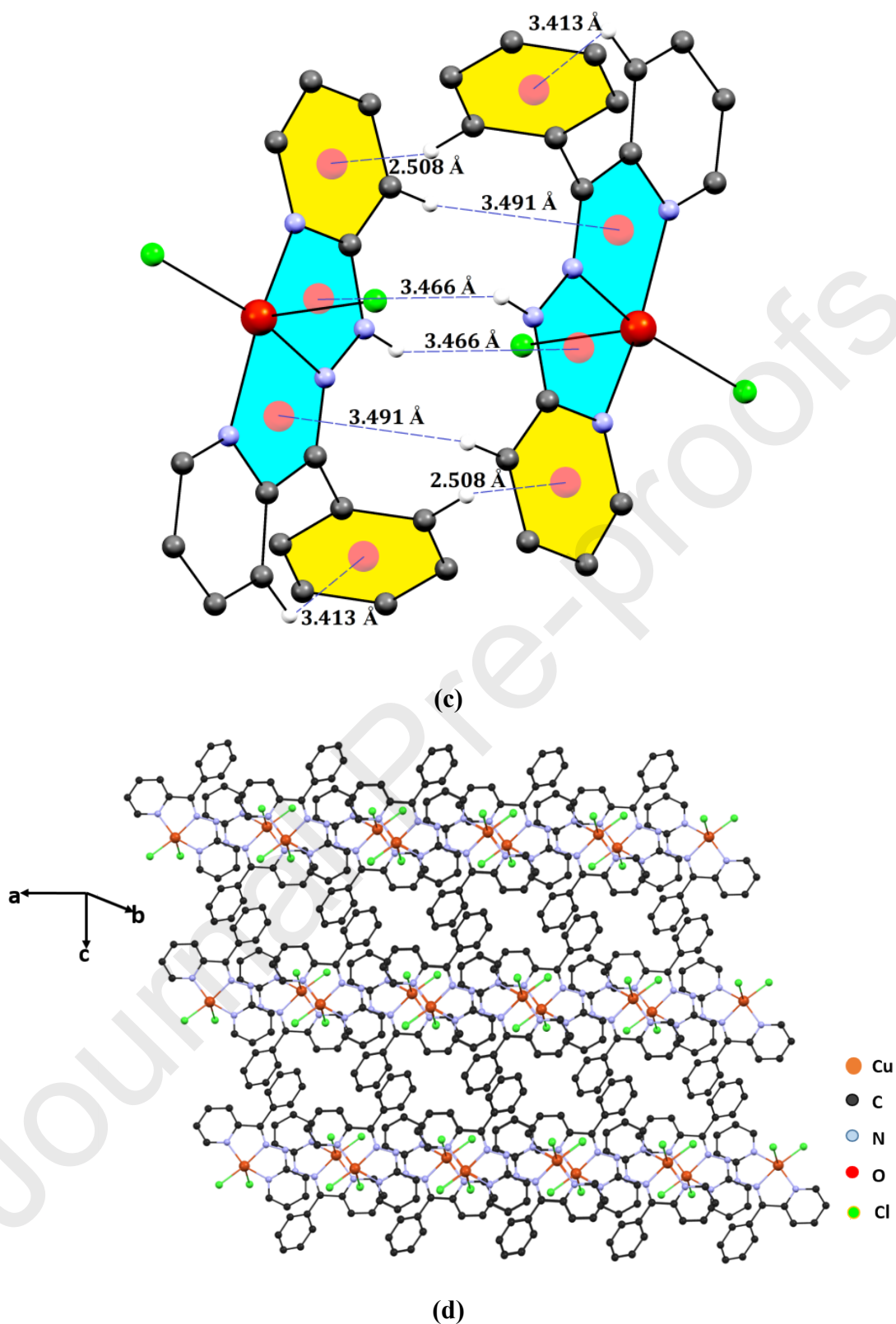


Fig. 1 (a) Molecular structure of complex **1**, (b) the co-former HIm interaction with the hydrogen bonded motif in **1**, (c) C – H \cdots π (metal chelate) interactions, (d) stereoscopic view of the cell of complex **1** down the b-axis (the a-axis is vertical).

The molecular structure of complex **1** consists of a discrete mononuclear [CuL(Cl₂)] unit. A perspective view of the structure, together with the atom labelling scheme of complex **1**, is shown in Fig. 1a. The copper(II) ion is five coordinated with a geometry that is intermediate between a trigonal bipyramid (c_{3v}) and a square-based pyramid (c_{4v}¹). The distortion in the geometry is described by Addison and his coworker.⁴⁴ According to the procedure for the Addison parameter (τ_5), the copper(II) atom has a τ value of 0.088 ($\tau_5 = \frac{(\beta - \alpha)}{60}$, where β and α are the largest angles in the coordination sphere), thus the coordination environment can be better described as a distorted square pyramidal structure in which the four-fold polyhedron is comprised of the N1, N2, N3 and C11 atoms, with the axial atom Cl2. The Cu-Cl2 bond length is longer than equatorial bonds, which results from the Jahn-Teller effect. The slight distortion in the basal plane of the coordination polyhedron may be due to the strain imposed by the Schiff base to the copper(II) center during coordination. The axially coordinated Cl2 atom has longer bond distance [2.5116(6) Å] than equatorially coordinated C11 [2.2429(5) Å] atom. The copper(II) ion is shifted by 0.249 Å towards the axially bound Cl2 atom from the basal plane. In addition to H-bonding, various C-H $\cdots\pi$ (aryl or metal chelates) interactions are detected, having ring centroid (H \cdots C_g) distances in the range 2.508-3.491 Å (Fig. 1c). The C-H $\cdots\pi$ interactions are responsible for extra stabilization in the solid-state. The axially coordinated Cl2 atom is involved in a hydrogen bond interaction with the H atoms of an adjacent molecule. The involved Cl2 atom showed bifurcated interactions, thus forming two R₂¹(6) membered heterosynthons (Fig. 1b). The hydrogen bond parameters are presented in Table 3. The two R₂¹(6) motifs are responsible for the formations of a homodimer. The intermolecular C-H $\cdots\pi$ (aryl and metal chelate) interactions are also responsible for the formation of the homodimer (two co-crystals).

Table 1. Crystal data and structure refinement for complexes **1** and **2**.

	1	2
Empirical formula	C ₁₇ H ₁₄ Cl ₂ CuN ₄	C ₆₈ H ₈₀ Cu ₄ N ₁₆ O ₂₈ S ₄
Formula weight	408.76	1951.88
Temperature (K)	100(2)	100(2)
Wavelength (Å)	0.71073	0.71073
Crystal system	Triclinic	Triclinic
Space group	<i>P</i> - <i>1</i>	<i>P</i> - <i>1</i>
a (Å)	8.4475(3)	8.2118(2)
b (Å)	9.6940(3) Å	14.8543(3)
c (Å)	11.4276(3) Å	17.2565(4)
α (°)	93.352(2)	74.1250(10)
β (°)	110.877(2)	80.5990(10)
γ (°)	105.187(2)	74.2080(10)
Volume (Å ³)	831.78(5)	1939.25(8)
Z	2	1
Density (calculated) (Mg/m ³)	1.632	1.671

Absorption coefficient (mm ⁻¹)	1.640	1.284
F(000)	414	1004
Crystal size (mm ³)	0.23 x 0.16 x 0.12	
Theta range for data collection (°)	2.652 to 33.256	2.547 to 28.328
Index ranges	-13<=h<=13, -14<=k<=14, -17<=l<=17	-10<=h<=10, -19<=k<=19, -23<=l<=23
Reflections collected	23733	28965
Independent reflections	6350 [R(int) = 0.0594]	9599 [R(int) = 0.0212]
Completeness to theta = 25.242°	99.9 %	99.8 %
Refinement method	Full-matrix least-squares on F ²	Full-matrix least-squares on F ²
Data / restraints / parameters	6350 / 0 / 217	9599 / 0 / 597
Goodness-of-fit on F ²	1.058	1.062
Final R indices [I>2sigma(I)]	R1 = 0.0426, wR2 = 0.0918	R1 = 0.0252, wR2 = 0.0614
R indices (all data)	R1 = 0.0665, wR2 = 0.1008	R1 = 0.0307, wR2 = 0.0649
Largest diff. peak and hole (e Å ⁻³)	1.124 and -1.049	0.428 and -0.490

Table 2. Bond lengths [Å] and angles [°] for complexes **1** and **2**.

1					
Bond lengths					
	XRD data	DFT data		XRD data	DFT data
Cu-N(3)	1.9856(16)	1.9856	Cu-Cl(1)	2.2429(5)	2.2429
Cu-N(1)	2.0065(17)	2.0065	Cu-Cl(2)	2.5116(6)	2.5116
Cu-N(4)	2.0177(18)	2.0177			
Bond angles					
N(3)-Cu-N(1)	79.14(7)	79.14	N(4)-Cu-Cl(1)	98.35(5)	98.35
N(3)-Cu-N(4)	79.33(7)	79.36	N(3)-Cu-Cl(2)	96.27(5)	96.27
N(1)-Cu-N(4)	155.75(7)	156.13	N(1)-Cu-Cl(2)	95.15(5)	95.18
N(3)-Cu-Cl(1)	161.04(5)	161.38	N(4)-Cu-Cl(2)	98.15(5)	98.23
N(1)-Cu-Cl(1)	98.39(5)	98.39	Cl(1)-Cu-Cl(2)	102.68(19)	103.69
2					
Bond lengths					
Cu(1)-O(1A)	1.9303(11)	1.9303	Cu(2)-O(1B)	1.9214(11)	1.9214
Cu(1)-N(3A)	1.9557(13)	1.9557	Cu(2)-N(3B)	1.9593(13)	1.9601
Cu(1)-N(1A)	2.0087(13)	2.0086	Cu(2)-N(1B)	2.0032(13)	2.0032
Cu(1)-N(4A)	2.0136(13)	2.0136	Cu(2)-N(4B)	2.0163(13)	2.0163
Cu(1)-O(1A)#1	2.2806(11)	2.2806	Cu(2)-O(1W)	2.1841(12)	2.1841
Sulfur ion					
S(1)-O(2A)	1.4538(11)	1.4538	O(1B)-S(2)	1.5029(11)	1.5031
S(1)-O(4A)	1.4653(11)	1.4652	O(2B)-S(2)	1.4685(12)	1.4685
S(1)-O(3A)	1.4684(11)	1.4684	O(3B)-S(2)	1.4714(12)	1.4714
S(1)-O(1A)	1.5400(11)	1.5399	O(4B)-S(2)	1.4697(12)	1.4697
Bond angles					
O(1A)-Cu(1)-N(3A)	176.68(5)	176.68	O(1B)-Cu(2)-N(3B)	173.08(5)	173.08
O(1A)-Cu(1)-N(1A)	103.74(5)	103.89	O(1B)-Cu(2)-N(1B)	97.29(5)	97.29
N(3A)-Cu(1)-N(1A)	79.57(5)	79.57	N(3B)-Cu(2)-N(1B)	79.53(5)	79.53
O(1A)-Cu(1)-N(4A)	97.11(5)	97.11	O(1B)-Cu(2)-N(4B)	101.95(5)	102.31
N(3A)-Cu(1)-N(4A)	79.58(5)	79.58	N(3B)-Cu(2)-N(4B)	80.02(5)	80.02
N(1A)-Cu(1)-N(4A)	157.67(5)	158.37	N(1B)-Cu(2)-N(4B)	157.36(5)	158.11
O(1A)-Cu(1)-O(1A)#1	78.59(5)	78.59	O(1B)-Cu(2)-O(1W)	89.11(5)	89.24
N(3A)-Cu(1)-O(1A)#1	101.25(5)	101.25	N(3B)-Cu(2)-O(1W)	97.50(5)	97.50
N(1A)-Cu(1)-O(1A)#1	99.58(5)	99.58	N(1B)-Cu(2)-O(1W)	100.44(5)	100.44
N(4A)-Cu(1)-O(1A)#1	92.24(5)	92.24	N(4B)-Cu(2)-O(1W)	91.74(5)	91.74
Sulfur ion					
O(2A)-S(1)-O(4A)	111.95(7)	111.95	O(2B)-S(2)-O(4B)	111.63(7)	111.63
O(2A)-S(1)-O(3A)	112.77(7)	112.77	O(2B)-S(2)-O(3B)	110.98(7)	110.98
O(4A)-S(1)-O(3A)	111.41(7)	111.41	O(4B)-S(2)-O(3B)	109.98(7)	109.98
O(2A)-S(1)-O(1A)	107.66(7)	106.84	O(2B)-S(2)-O(1B)	109.38(7)	109.59
O(4A)-S(1)-O(1A)	106.30(7)	106.30	O(4B)-S(2)-O(1B)	107.22(7)	107.22
O(3A)-S(1)-O(1A)	106.30(6)	106.30	O(3B)-S(2)-O(1B)	107.48(7)	107.48

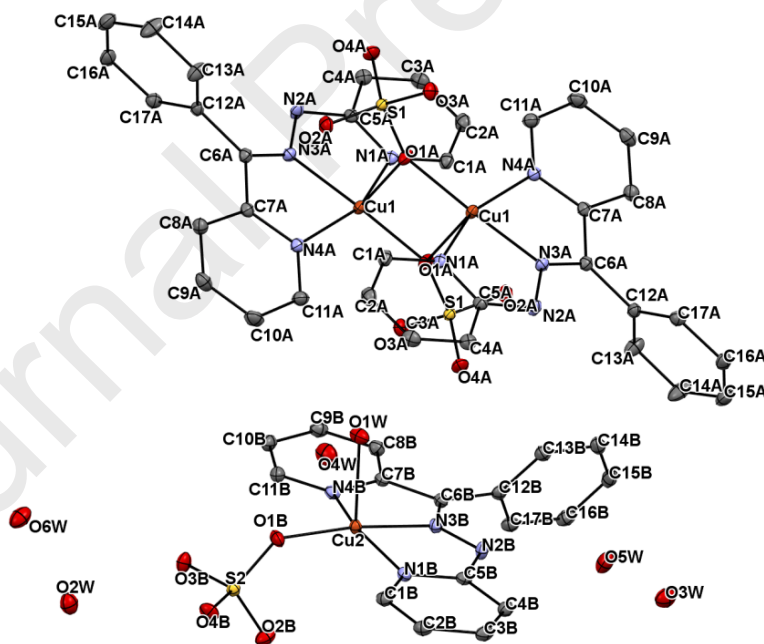
Symmetry transformations used to generate equivalent atoms: #1 -x+1,-y+1,-z+1

Table 3. Hydrogen bonds [Å and °] for complexes **1** and **2**.

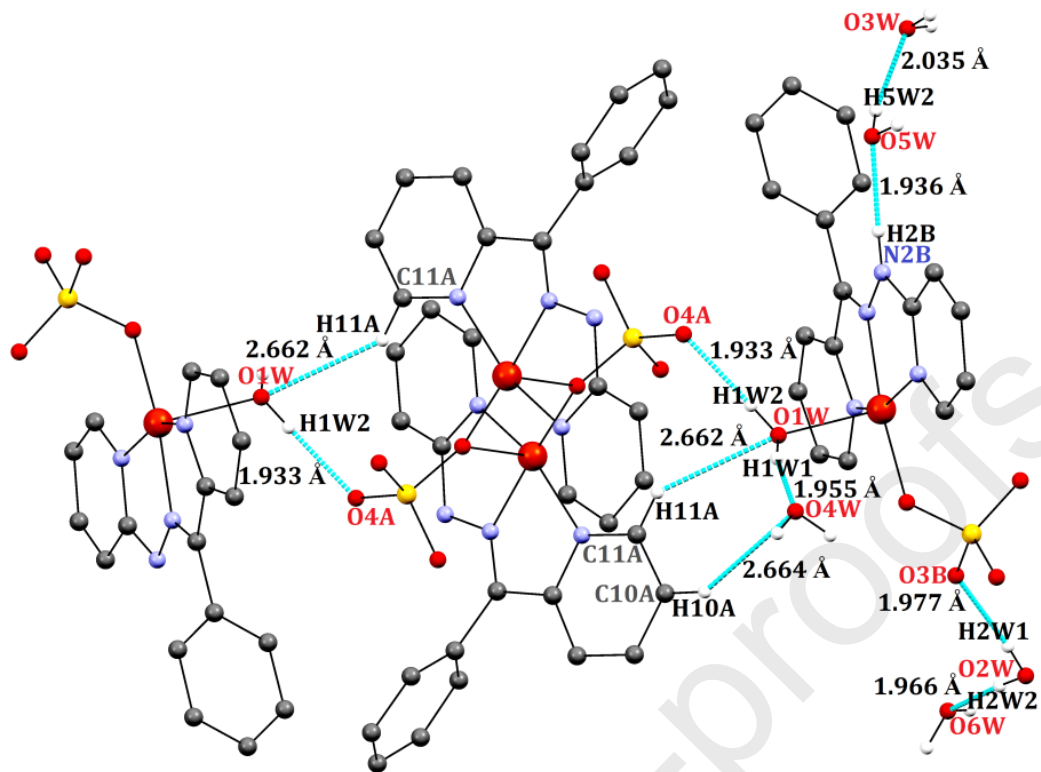
D-H...A	d(D-H)	d(H...A)	d(D...A)	<(DHA)	Symmetry transformations
1					
N(2)-H(2B)...Cl(2)#1	0.88	2.37	3.1579(16)	149.6	#1 -x+1,-y+1,-z+1
C(1)-H(1A)...Cl(1)	0.95	2.84	3.392(2)	117.8	
C(4)-H(4A)...Cl(2)#1	0.95	2.78	3.531(2)	136.8	
C(16)-H(16A)...Cl(1)#2	0.95	2.73	3.669(2)	168.6	#2 -x,-y+2,-z+1
C(17)-H(17A)...Cl(1)	0.95	2.90	3.428(2)	116.4	
2					
N(2A)-H(2A)...O(3A)#1	0.83(2)	1.97(2)	2.7291(17)	153(2)	#1 -x+1,-y+1,-z+1
C(1A)-H(1AA)...O(2A)	0.95	2.48	3.360(2)	153.6	
C(4A)-H(4AA)...O(3A)#2	0.95	2.57	3.1928(19)	123.7	#2 -x,-y+1,-z+1
O(1W)-H(1W1)...O(4W)	0.82(2)	1.96(2)	2.7573(19)	167(2)	
O(1W)-H(1W2)...O(4A)	0.81(3)	1.93(3)	2.7382(17)	177(3)	
N(2B)-H(2B)...O(5W)	0.82(2)	1.94(2)	2.7460(19)	168(2)	
C(2B)-H(2BA)...O(3B)#3	0.95	2.59	3.253(2)	127.0	#3 x+1,y,z
C(10B)-H(10B)...O(4W)#4	0.95	2.56	3.406(2)	148.9	#4 x-1,y,z
C(11B)-H(11B)...O(3B)	0.95	2.56	3.403(2)	147.8	
O(2W)-H(2W1)...O(3B)	0.78(3)	1.98(3)	2.7596(18)	175(2)	
O(2W)-H(2W2)...O(6W)	0.81(3)	1.97(3)	2.767(2)	171(3)	
O(3W)-H(3W1)...O(4B)#5	0.80(3)	1.99(3)	2.7832(18)	172(3)	#5 -x+1,-y+2,-z
O(3W)-H(3W2)...O(2W)#6	0.80(3)	2.03(3)	2.8173(19)	168(3)	#6 -x,-y+2,-z
O(4W)-H(4W1)...O(6W)#3	0.84(3)	2.05(3)	2.874(2)	166(3)	
O(4W)-H(4W2)...O(2W)#7	0.82(3)	2.09(3)	2.8720(19)	159(3)	#7 -x+1,-y+1,-z
O(5W)-H(5W1)...O(2B)#5	0.77(3)	2.05(3)	2.8268(18)	177(3)	
O(5W)-H(5W2)...O(3W)	0.77(3)	2.03(3)	2.774(2)	161(3)	
O(6W)-H(6W1)...O(4B)#4	0.79(3)	2.01(3)	2.7824(19)	164(3)	
O(6W)-H(6W2)...O(3B)#8	0.84(3)	1.98(3)	2.8051(18)	169(3)	#8 -x,-y+1,-z

The single crystal X-ray structures were determined for all co-crystals for a better understanding of the molecular packing and the non-covalent interactions amongst the molecules, in particular the supramolecular architectures. The molecular structure of **2** reveals co-crystals of monomer and binuclear copper(II) complexes in a 1:1 ratio. The binuclear co-crystal of complex **2** has a noncentrosymmetric structure with a binuclear $\text{Cu}_2(\text{Cu-O-R})_2$ rectangular core. One oxygen atom of the sulfate anion acts as a bridge between two copper(II) metal centers. The coordination geometry around each copper(II) center is distorted pyramidal. The relative amounts of the distortion of the square pyramids are given by the Addison factor (τ_5).⁴⁵ The τ_5 values for two copper(II) centers are estimated as $(\tau_5)_1 = 0.3$ and $(\tau_5)_2 = 0.2$. Thus, the coordination environment of each copper(II) center is a slightly distorted square pyramidal structure in which the four equatorial sites are comprised of O(1A), N(3A), N(1A) and N(A) atoms, with the axial position being occupied by one of the oxygen atoms of the sulfate anion which also coordinates to the second copper(II) center, acting as bridging ligand. In the binuclear motif, the $\text{Cu}\cdots\text{Cu}$ distance is 3.266 Å. The two copper atoms are separated by 1.930 Å through the bridging oxygen atoms of the sulfate anions, with $\text{Cu}(\text{M-O})\text{-Cu}$ angles of 101.41 and 89.10 °, respectively. The values of these angles exhibit anti-ferromagnetic coupling. The copper(II)-copper(II) distance is within the usual range for this type of complex^{46,47}. The monomer unit of this binuclear complex is shown in Fig. 2. The coordination environment of the copper(II) center is distorted square pyramidal as suggested by the τ_5 factor ($\frac{\beta - \alpha}{60^\circ}$

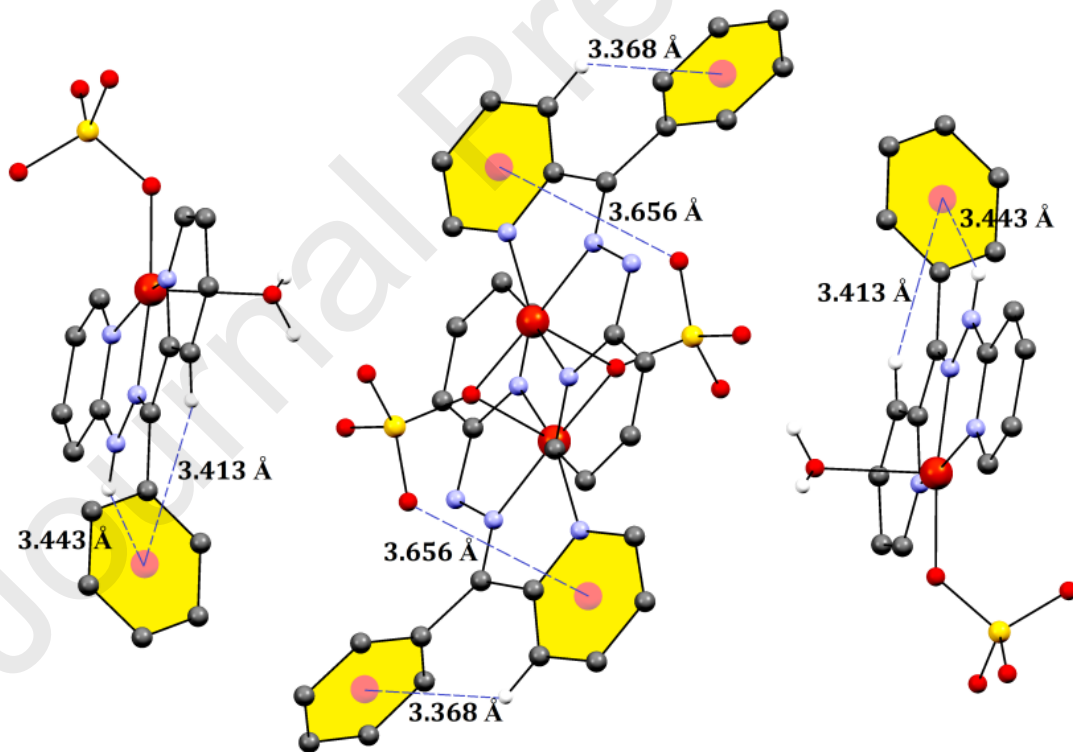
). The less distortion is consistent with the crystallographically imposed symmetry (the plane comprised of the N1B, N3B, N3B and O1B atoms), since the equatorial plane of the complex is formed by these donor atoms together with a long axial Cu(2)-O1W bond. The guest mononuclear motif has pentacoordination around the copper(II) center. Selected bond lengths and bond angles are presented in Table 2. The basal plane of the copper center comprises two pyridine nitrogen atoms and one azo nitrogen atom of L⁻. One perchlorate anion takes the fourth position of the basal plane. The axial position of the metal coordination sites is occupied by one oxygen atom of a water molecule. Thus, the geometry of the copper ion in this motif can be described by a square pyramidal structure in which the c_4 axis is composed of the N1B, N3B, N4B and O1B atoms. The relative amount of the square pyramidal component is indicated by τ_5^{48} . The value of τ_5 is 0.262, which describes a distorted square pyramidal geometry. The Cu2-O1W bond length is the longest compared to the distances from the Cu center to the other atoms, a fact which is consistent with the O1W atom being the apex of the pseudo square pyramid, allowing for Jahn-Teller distortion.



(a)



(b)



(c)

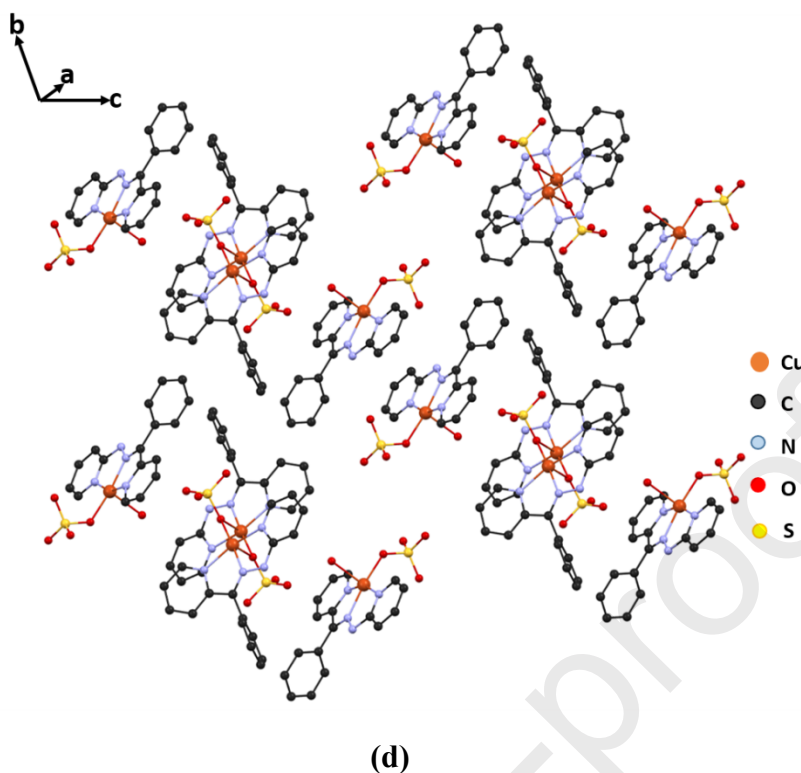


Fig. 2 (a) Molecular structure of **2**, (b) the interaction with the hydrogen bonded motif in stoichiometric co-crystals, (c) intermolecular C-H \cdots π (metal chelate) interactions, (d) stereoscopic view of the cell of complex **2** down the b-axis (the a-axis is vertical).

The arrangement of the two species present in the lattice structure allows a certain degree of hydrogen bonding throughout the crystal (Fig. 2b). The binuclear unit and two mononuclear units present a double interaction (intermolecular H-bonding) through the H-atom of an axially coordinated water molecule, H1W2 \cdots O1A (dHA = 1.933 Å). Similarly, a phenyl ring of the Schiff base forms H-bonding with the oxygen atom of coordinated water molecules of the monomer of the type C11A-H11A \cdots O1W (dHO = 2.662 Å). There are also several intermolecular hydrogen bonding interactions involving O/H atoms of water molecules with O atoms of the sulfate anion or the Schiff base atoms. All kinds of interaction parameters are presented in Table 3. In complex **2**, the interesting features of the structure are the formation of a supramolecular assembly through H-bonding interactions of coordinated/uncoordinated sulfate anions and water molecules. The hydrogen atoms, H and ..H attached to C, (C_g1) are involved in intermolecular C – H \cdots π (aryl) interactions and the H-atoms of H.....(C_g1) and H....(C_g2), attached to C atoms, are involved in intermolecular S – H \cdots π interactions with the ring centroid (H...C_g) of the binuclear complex. The CH \cdots π interactions, along with other H-bonding interactions, contribute extra stabilization to the solid-state. A stereoscopic

projection of the molecular arrangement within the unit cell along the b-axis is shown in Fig. 2d. The two monomers and one dimer unit constitute a 1D pattern.

3.3. Electronic spectra

The electronic spectra were recorded using DMSO (3.0×10^{-3} M) solutions of **1** and **2**. UV-visible absorption spectroscopy is a useful technique that has been frequently explored to provide structural information. A strong absorption band in the electronic spectra of complexes **1** and **2** at 278 nm was attributed to the $\pi\text{-}\pi^*$ transition of the aromatic rings and azomethine groups. The absorption band at 385 nm is due to a ligand to metal charge transfer (LMCT) from the $>\text{C}=\text{N}$ group to the copper(II) center⁴⁹. Furthermore, the complexes exhibit a copper-based $d\text{-}d$ band at ~ 580 nm and the transition occurs from ${}^2\text{E}_g \rightarrow {}^2\text{T}_{2g}$ ⁵⁰. The spectral properties of both complexes are very similar (Fig. 3).

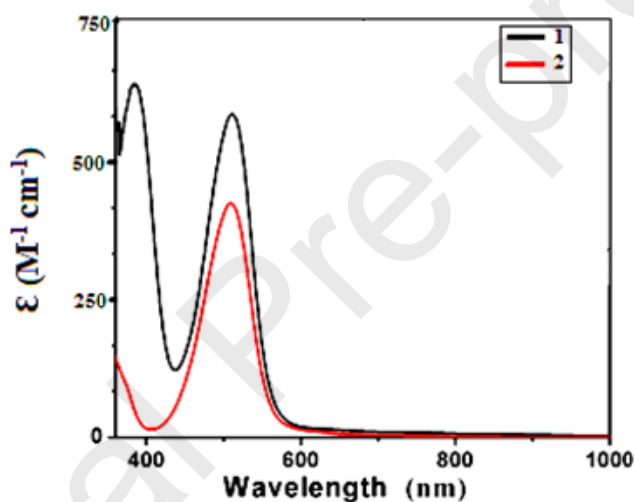


Fig. 3. UV-visible spectra of the copper(II) complexes **1** and **2** in DMSO solution, 3.0×10^{-3} M.

3.4. Electrochemical studies

The electrochemical behavior of both complexes was studied using cyclic voltammetry (CV) and differential pulse voltammetry (DPV) techniques. The CV and DPV diagrams are shown in Fig. 4. Both complexes display two reduction peaks at +0.21 ($\text{Cu}^{2+} \rightarrow \text{Cu}^{+1}$) and -0.34 V ($\text{Cu}^{+1} \rightarrow \text{Cu}^0$) for **1** and at -0.20 ($\text{Cu}^{2+} \rightarrow \text{Cu}^{+1}$) and -0.27 ($\text{Cu}^{+1} \rightarrow \text{Cu}^0$) for **2**, and one oxidation peak at -0.28 V ($\text{Cu}^0 \rightarrow \text{Cu}^{2+}$) for **1** and -0.15 V ($\text{Cu}^0 \rightarrow \text{Cu}^{2+}$) for **2**. This may be due to the chemical oxidation of copper during the complexation processes i.e. during the complexation processes the Cu^{+1} species is transformed into Cu^{2+} species and the ligand is reduced at a more negative potential (Fig. 4). On increasing the scan rate, the peak currents increase linearly, supporting the diffusion effect of the electrochemical (E_c) mechanism⁵¹. Both complexes show two reduction processes ($\text{Cu}^{\text{II}}\text{Cu}^{\text{II}} + \text{e}^- \rightarrow$

$\text{Cu}^{\text{II}}\text{Cu}^{\text{I}}$ and $\text{Cu}^{\text{II}}\text{Cu}^{\text{I}} + e^- \rightarrow \text{Cu}^{\text{I}}\text{Cu}^{\text{I}}$ vs AgCl references, both involving an identical number of electrons, as revealed from the differential pulse voltammography (DPV) experiments. The value of the second reduction potential of **2** is less negative than that of **1**, but the first reduction potential values are nearly identical. Such a less negative reduction potential may be attributed due to the high molecular weight of **2**. The DPV technique is a very good electrochemical technique for resolving reduction peak potentials with small differences in peak potentials (180 mV)⁵². This technique further supports the existence of two reduction processes (Fig. 4b) and is also in agreement with the foregoing results⁵³.

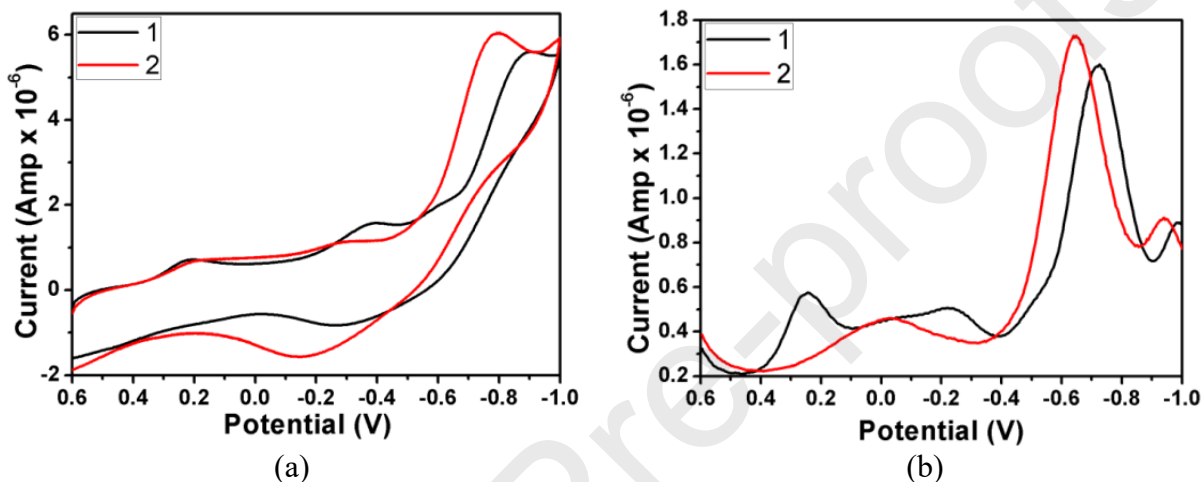


Fig. 4. (a) Cyclic voltammograms of complexes **1** and **2** in DMSO at an Ag/AgCl electrode with a scan rate of 300 mV s⁻¹ and a temperature of 20 °C. (b) Differential pulse voltammogram of complexes **1** and **2** at room temperature using a scan rate of 20 mV s⁻¹ in DMSO. The pulse amplitude is 50 mV.

3.5. EPR measurements

The EPR spectra of complexes **1** and **2** were recorded with a Varian E-line spectrometer working in the X-band using polycrystalline samples at RT and in DMSO solution (3×10^{-3} M) at liquid nitrogen temperature (LNT) (Fig. 5). The EPR spectra of the complexes in the polycrystalline form are typical for the triplet state ($S=1$). The polycrystalline room temperature spectra of both complexes are found without any hyperfine structure. The signal (half field) for $\Delta M_s = \pm 2$ is weak for both complexes. The occurrence of such a dimeric triplet state in **1** is due to dipole-dipole interactions. Such interactions are responsible for the formation of the dimer, which has already been explained in the single-crystal X-ray discussion. In complex **1**, the dipole-dipole interactions survive in DMSO solution at LNT (Fig. 5), whereas complex **2** decomposed in DMSO, yield spectral features of the mononuclear complex. In the binuclear complexes **2** ($\Delta M_s = \pm 2$) signals were found, although in the sulfato bridged complex they are weak. The polycrystalline spectra are similar in

appearance, with g_{\parallel} and g_{\perp} signals. The values in the polycrystalline state are $g_{\parallel} = 2.216$, $g_{\perp} = 2.067$, $G = 2.56$ and $g_{\parallel} = 2.190$, $g_{\perp} = 2.072$, $G = 2.93$ for complexes **1** and **2**, respectively. The exchange interaction parameter G of the complexes suggests that there is an interaction ($G < 4$) between the two copper centers. $\Delta M_s = \pm 2$ is strong in complex **2**. These observations are in agreement with the antiferromagnetic interaction between copper ions in both complexes⁵⁴. The frozen DMSO solution yielded the parameters $g_{\parallel} = 2.219$, $g_{\perp} = 2.063$ and $A_{\parallel} = 167$ G for complex **1**. The nearly axial character of the g -tensor, with $g_{\parallel} > g_{\perp} > 2.023$, indicates that the ground state arises from a $d_{x^2-y^2}$ orbital, which is in agreement with $\tau_5 = 0.262$ for the square pyramidal coordination sphere⁵⁵. Such broad band features are consistent with the magneto-chemical properties, which indicated a spin-spin interaction⁵⁶. The frozen solution EPR spectrum of complex **2** shows four lines, typical of copper(II) ions ($I = 3/2$), as a result of the hyperfine interaction between the unpaired electrons and copper(II) center. The values $g_{\parallel} = 2.284$, $g_{\perp} = 2.057$ and $A_{\parallel} = 167$ G were obtained. As $g_{\parallel} > g_{\perp}$, a square pyramidal geometry can be proposed for the copper(II) centers. Such observations are suggestive of dissociation of this complex into two mononuclear copper(II) species.

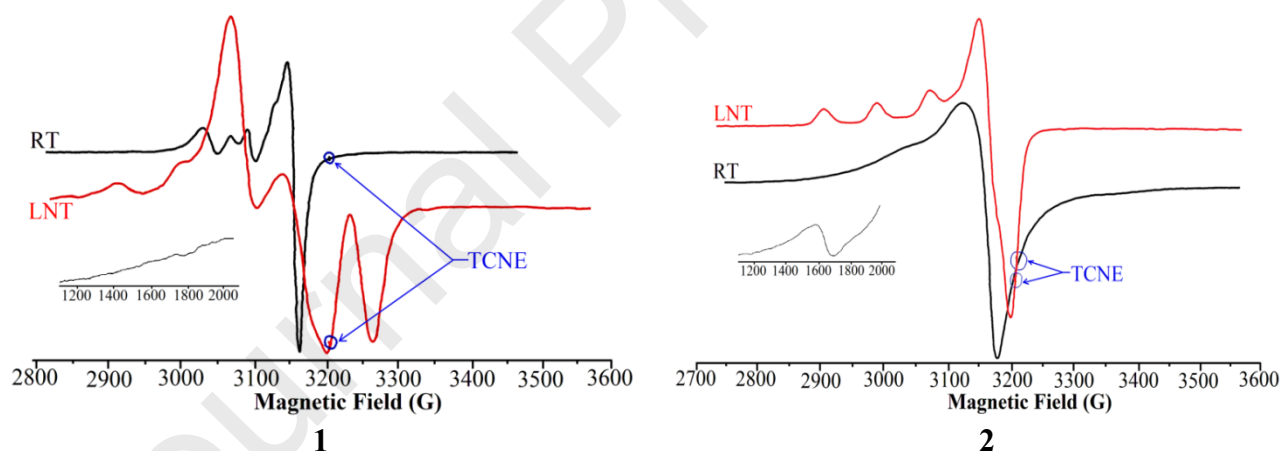


Fig. 5. X-band EPR spectra of complexes **1** and **2** in the polycrystalline state (RT) and DMSO solution at LNT. Inset: EPR spectra showing half-field signals.

3.6. Thermal gravimetric analysis

The thermal behavior of the complexes was studied by thermal gravimetric analysis. The curves of the thermo-gravimetric analysis (TG) are displayed in Fig. 6. Thermal decomposition of the copper complexes occurs in the temperature range 100-530 °C, showing the high thermal stability of the complexes. The thermal decomposition process occurs in two steps and three steps for complex **1** and **2**, respectively, as shown in Scheme 4. In the TG graph of complex **1**, the weight loss at 250-360 °C

is associated with the separation of the ligand molecule, while the next step, with a weight loss at 400-500 °C, is attributed to the loss of the Cl₂ moieties, leaving behind CuO as the final product. In the TG graph of complex 2, thermal dehydration of the complex occurs in the range 100-200 °C, due to the loss of the water molecules. In the next step, loss of the ligand takes place, at 280-370 °C, while in the final step, a weight loss occurs in the range 400-500 °C due to the removal of the SO₄ molecule. Copper oxide CuO, which is stable up to 514 °C, was obtained as the final product⁵⁷⁻⁵⁹.

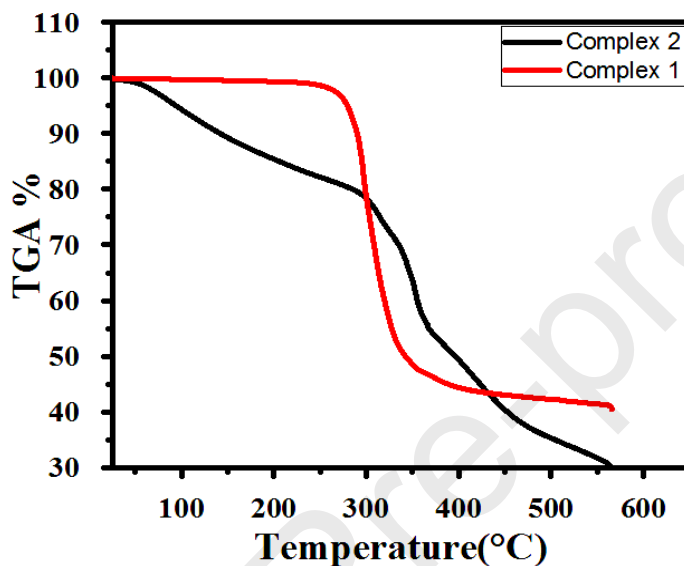
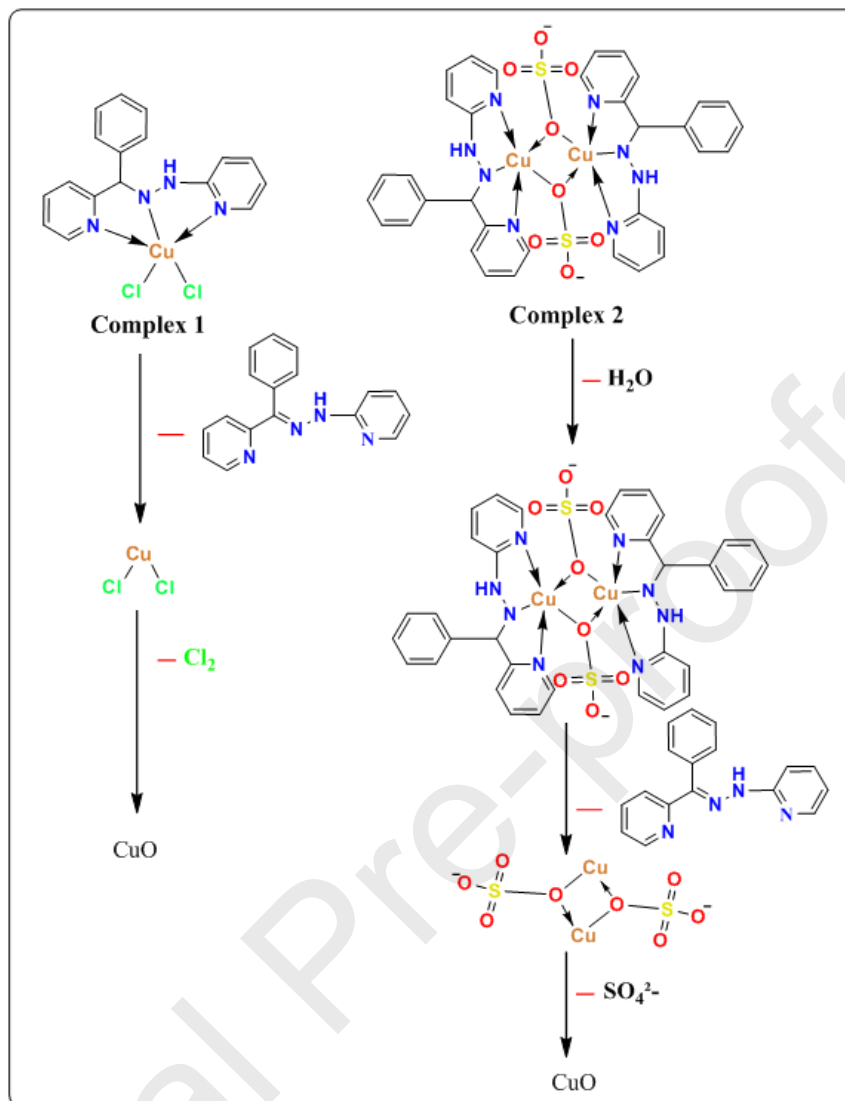


Fig. 6. TGA curves of complexes 1 and 2.



Scheme 4. TG decomposition pattern of the complexes.

3.7. Cryomagnetic susceptibility studies

The thermal variation of $\chi_M T$ (χ_M = molar magnetic susceptibility) for complexes **1** and **2** over the temperature range 300-2 K is shown in Fig. 7. The value of the $\chi_M T$ product obtained at room temperature for complex **1** is $0.43 \text{ cm}^3 \text{ K mol}^{-1}$, which is slightly larger than the value expected for an isolated $S = \frac{1}{2}$ copper(II) ion ($0.375 \text{ cm}^3 \text{ K mol}^{-1}$). On cooling, the $\chi_M T$ product remains roughly constant until approximately 45 K when a slight decrease in this value is observed. Further cooling of the sample leads to a sharper decrease in $\chi_M T$, which is ascribed to antiferromagnetic interactions (Fig. 7).

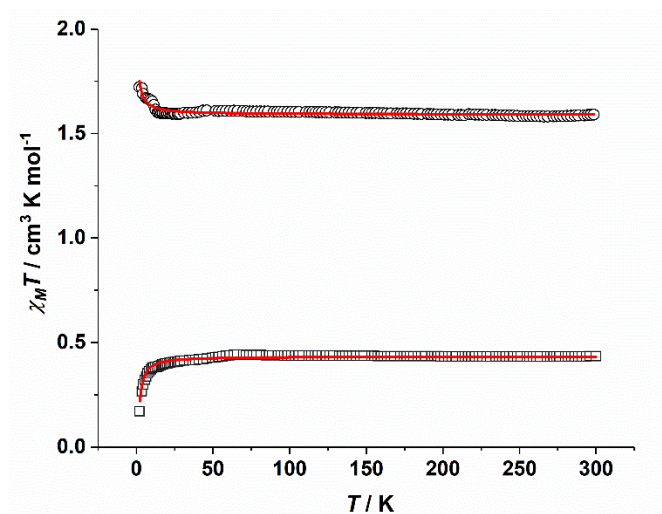


Fig. 7. Temperature dependence of the $\chi_M T$ product of complexes **1** (squares) and **2** (circles) measured under a magnetic field of 0.5 T. The solid lines represent the fit of the data as described in the text.

Taking into account the crystal structure of complex **1**, which is formed by mononuclear copper(II) species, it is reasonable to consider that the interactions occur through space and hydrogen bonds between the $S = \frac{1}{2}$ ions situated at the shortest intermolecular distances. It must be pointed out that although hydrogen bonds are medium-range interactions, they can strongly influence the magnetic properties of compounds in some cases⁶⁰. A view of the packing of the structure of **1** along the a -axis shows alternating intermolecular $\text{Cu}\cdots\text{Cu}$ distances of 4.031 and 6.595 Å that form an imaginary zigzag chain with a $\text{Cu}\cdots\text{Cu}\cdots\text{Cu}$ angle of 130.07°. Moreover, the structure displays hydrogen bonding between the mononuclear species, whose copper ions are placed at 6.595 Å (Fig. 8).

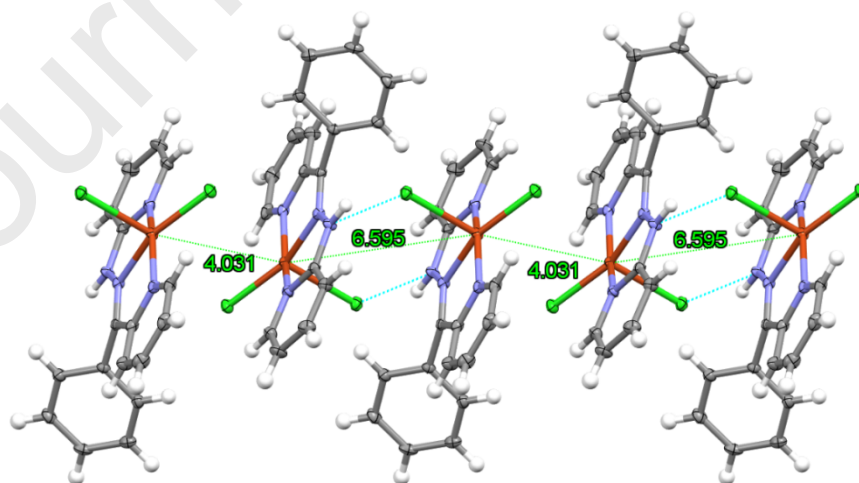


Fig. 8. View of complex **1** along the *a* crystallographic axis, showing the shortest intermolecular Cu···Cu distances (Å) and the hydrogen bonds between the mononuclear species.

In a first approach, the $\chi_M T$ data of **1** were fitted with an alternating Heisenberg linear chain model, whose spin Hamiltonian is as follows:

$$H = -J \sum_{i=1}^n [S_{2i} \cdot S_{2i-1} + \alpha S_{2i} \cdot S_{2i+1}],$$

where J is the exchange coupling constant and α takes into account the distortion in the chain with values ranging from $\alpha = 0$ (isolated dimers) to $\alpha = 1$ (uniform chain of $S = \frac{1}{2}$ spins). The analytical expression employed in the fit is:

$$\chi_M = \frac{Ng^2\beta^2}{kT} \frac{A + Bx + Cx^2}{1 + Dx + Ex^2 + Fx^3}$$

where N , g , β and k have their usual meanings, $x = |J| / kT$ and A-F are functions of α ⁶¹. The best parameters obtained were $g = 2.15$, $\alpha = 0.68$, and $J = -1.8 \text{ cm}^{-1}$ with $\sigma^2 = 5.77 \times 10^{-4}$ (Fig. 8). Therefore, antiferromagnetic coupling constants of -1.8 and -1.2 cm^{-1} along a 1D arrangement of $S = \frac{1}{2}$ spins have been deduced from this fit. Although the value of α suggests that there are no magnetically isolated dimers in the structure, the experimental data of **1** were fitted in a second approach with the Bleany-Bowers equation for comparison:

$$\chi_M = \frac{2Ng^2\beta^2}{3KT} \frac{3}{3 + \exp\left[-\frac{J}{KT}\right]}$$

(derived from the $H = -J S_1 \cdot S_2$ Hamiltonian)

The best fit of the data with this model led to g and J values of 2.16 and -3.2 cm^{-1} , respectively (Fig. S5). This model considers only one magnetic exchange pathway in the structure and a larger value of J in absolute value was obtained. The $\chi_M T$ product of **2** at room temperature is $1.66 \text{ cm}^3 \text{ K mol}^{-1}$. This value is close to the one expected ($1.50 \text{ cm}^3 \text{ K mol}^{-1}$) for the four $S = \frac{1}{2}$ copper(II) ions that comprise the structure of this compound. A Curie-like behavior is observed in the $300\text{-}15 \text{ K}$ range and an increase of the $\chi_M T$ value on lowering the temperature, ascribed to ferromagnetic interactions, is observed below 15 K (Fig. S5). The $\chi_M T$ vs T data were fitted using a model that takes into account the magnetic contribution of a copper(II) dimer through the Bleany Bowers equation (see above) and the contribution of two copper(II) monomers. Therefore, it has been considered that an intradimer ferromagnetic coupling is responsible for the magnetic behavior observed in **2**. The g value of the monomeric copper(II) ions was fixed to the value of 2 to obtain

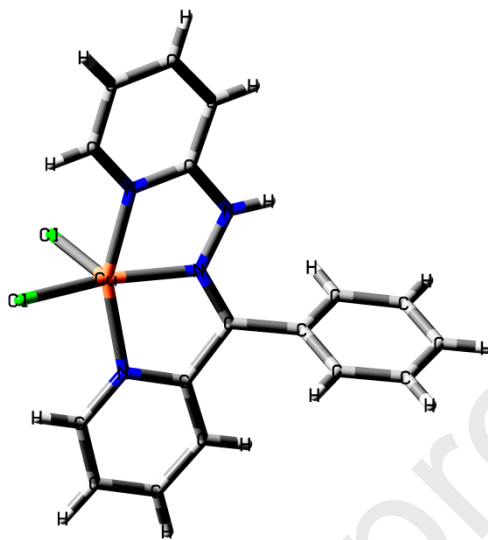
realistic values. The best data obtained from this fit were $g = 2.12$ and $J = 1.4 \text{ cm}^{-1}$, with $\sigma^2 = 1.08 \times 10^{-4}$.

A slightly distorted square-pyramidal coordination is observed for the two copper(II) ions that form the dimer of **2**. The copper(II) ions are double bridged by one oxygen atom of each of the two sulfate anions in the structure of the dimer. The dimer displays a Cu...Cu distance of 3.266 Å, Cu-O distances of 2.281 and 1.930 Å and Cu-O-Cu angle of 101.41 ° (see the structural characterization part for more information). These parameters are relevant because it is well known that antiferromagnetic or ferromagnetic interactions of very different magnitude can be observed in similar dimeric copper(II) complexes depending on the geometry, the τ parameter, the Cu-O-Cu angle, and the Cu-O and Cu...Cu distances⁶². However, it is frequent to observe opposed effects for these parameters and, indeed, it has been observed that it is particularly difficult to predict the sign and the value of the coupling constant in similar systems in which the copper(II) ions are double bridged, similarly to that found in **2**⁶³. Nevertheless, it must be pointed out that both complexes display antiferromagnetic interactions. To the best of our knowledge, this is the first example of a dimeric copper(II) complex in which two oxygen atoms of two sulfate anions mediate a ferromagnetic coupling.

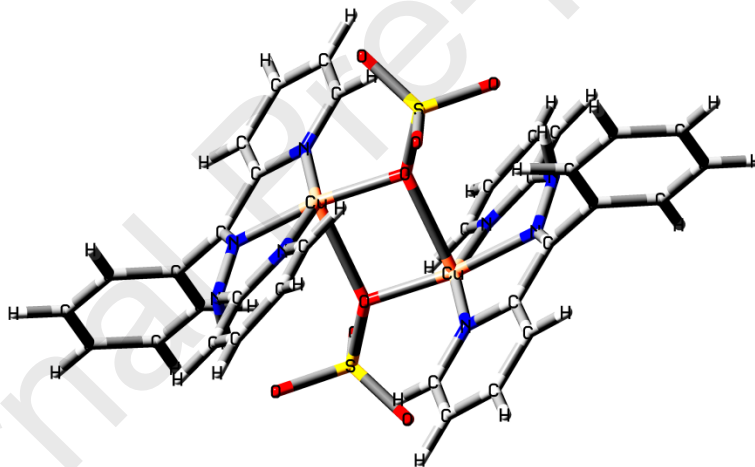
3.8. DFT calculations

To help with the physicochemical data (Epr and CV), DFT calculations were executed on complexes **1** and **2**. Geometry optimization was performed using density functional theory (DFT) at the B3LYP basic set^{64,65}. The optimized structures of the complexes are shown in Fig. 9. Analysis of the frontier molecular orbitals of the optimized structures shows that, in the gas phase, the highest occupied molecular orbitals (HOMOs) and lowest occupied molecular orbitals (LUMOs) of both complexes are similar in energy. The graphical representations (contour plots) of the frontier molecular orbitals (FMO) are depicted in Fig. 10. It is observed that the HOMOs of both complexes are mainly ligand centered, with the major contributions due to the p orbitals of the donor atoms. From these observations it is easy to find out why the electrochemical potential is equal in magnitude because the oxidation takes place on the coordinating tridentate ligand; the potentials are likely to be slightly influenced by the nature of bridging ligand. The HOMO-LUMO energies are descriptors that play an important role in deciding a wide range of chemical interactions⁶⁶. FMOs give an insight into the reactivity of complexes and active sites can be understood by the distribution of frontier orbitals. The theoretical transition level energy gap (ΔE) between the HOMO and LUMO is shown in Table 4.

On perusal of the HOMO-LUMO energy gap, it is observed that the gap (ΔE) is high in both complexes. This high ΔE value implies that energy is higher and a high chemical reactivity.



Complex 1



Complex 2

Fig. 9. Optimized structures of complexes 1 and 2.

Table 4. Molecular orbital energies and energy gap (ΔE).

Level	Molecular Orbital Energy (eV)		ΔE	
	1	2	1	2
HOMO	-3.896	-5.392		
LUMO	-1.008	-4.638	2.888	0.754
HOMO-1	-4.519	-6.335		
LUMO+1	+0.773	-2.808	3.746	3.527

LUMO	-5.025	-6.401		
LUMO+2	-0.728	-2.784	4.297	3.617

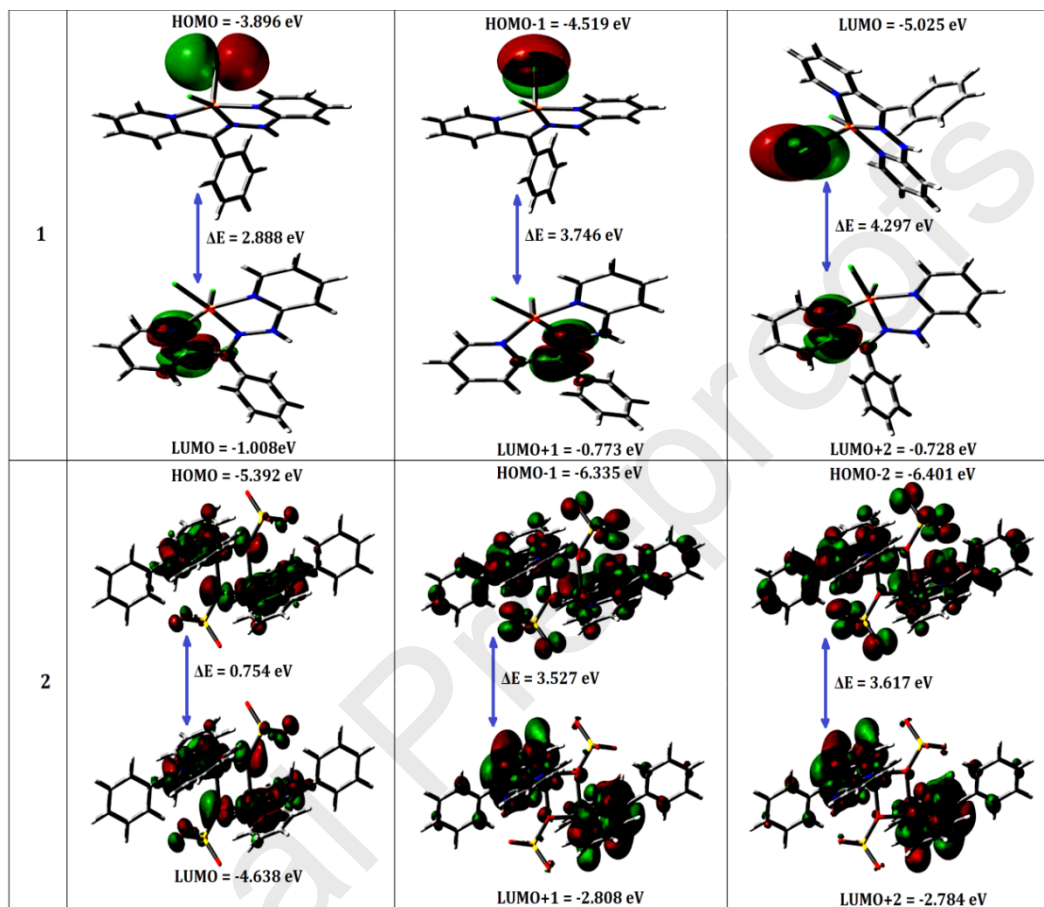


Fig. 10. HOMO-LUMO structures with the energy level diagrams.

The calculated spin densities were performed using the B3LYP/LANL2DZ as basis sets for both complexes. Fig. 10 illustrates the spin densities for the ground state. The spin density distributions are mainly delocalized on the copper atoms and those atoms which are directly coordinated to the copper atoms⁶⁷. The spin density plots of the complexes are shown in Fig. 11. The positive signed densities are spread over the metal center and the negative signed spin densities are distributed over the coordinated donor atoms. Such spin density distributions are also in agreement with the HOMO-LUMO shapes observed in both complexes. It is also shown from DFT calculations that the DFT data agree with the EPR spectral data, from which a mainly ligand centered character of

the unpaired electron in the $d_{x^2-y^2}$ orbital along with axial features of the EPR signals were concluded⁶⁸.

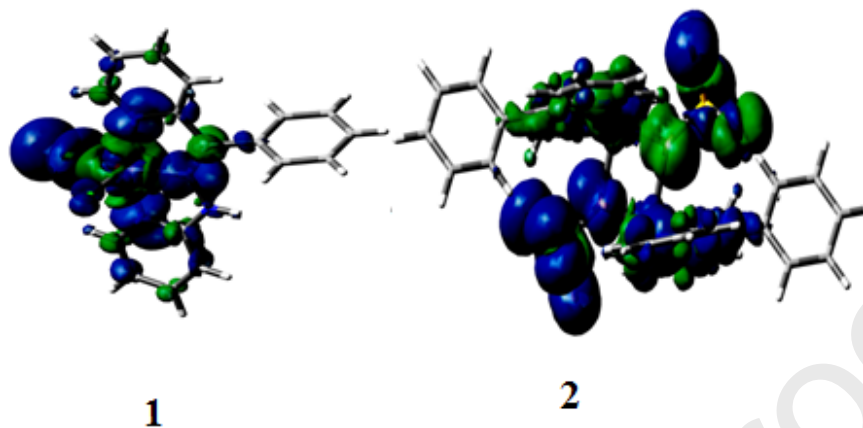


Fig. 11. Spin density plots of complexes **1** and **2**.

3.10. Natural bond order (NBO) analysis

NBO analysis of the synthesized complexes **1** and **2** has been carried out using the B3LYP/LAN2DZ basis set. The computed bond lengths and bond angles are explicitly similar to the experimentally observed values (Table 2). NBO analysis provides details about the natural charges between occupied Lewis-type orbitals and unoccupied non-Lewis NBOs (Rydberg), which correlates with the stabilizing donor-acceptor interactions^{69,70}. As per the NBO analysis, all the interactions for the Cu(II) ions and donor atoms are considered as coordination bonds ($N \rightarrow Cu$, $Cl \rightarrow Cu$ and $O \rightarrow Cu$). Such a type of interaction attributes to a donation of electron density from the lone pair orbital on the donor atoms (N/Cl/O), LP(Cl) or LP(O) to the anti-bonding orbital on the Cu(II) $LP^*(Cu)$. The involved selected orbitals in the interaction are shown in Fig. 12.

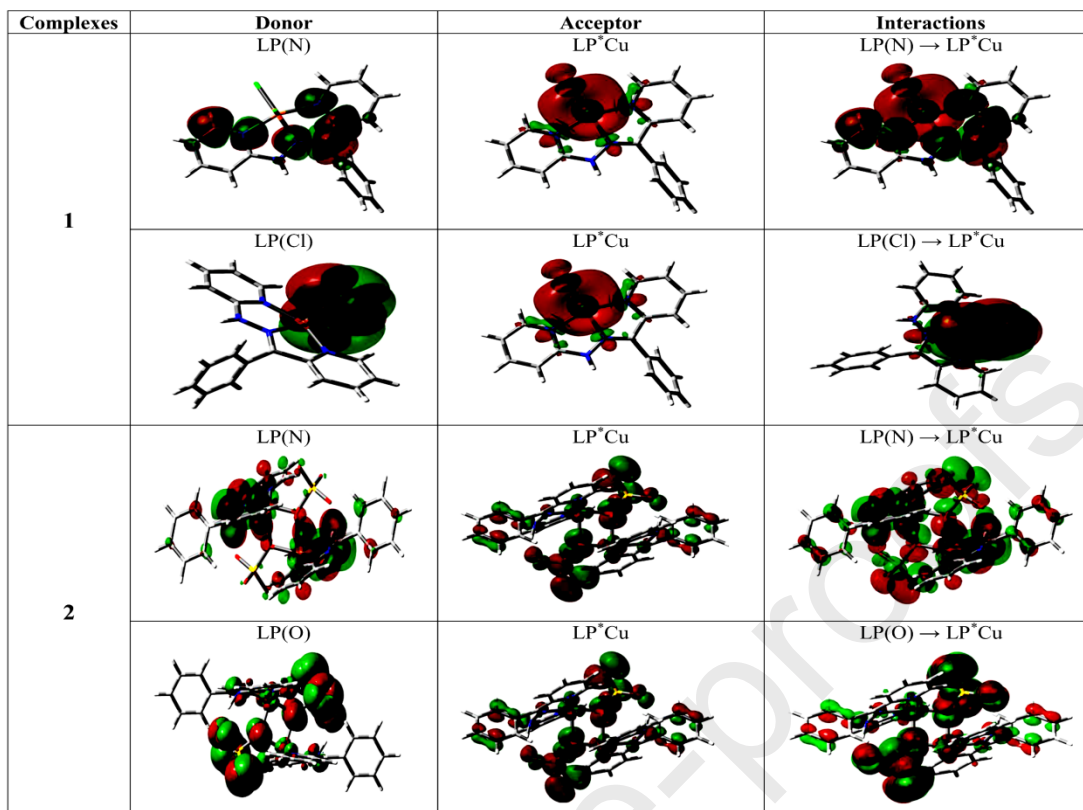


Fig. 12. The donor and acceptor orbitals involved in the LP(N)/ LP*(Cu) and LP(O)/ LP*(Cu) interactions.

The natural electronic configurations of the Cu atoms are [Ar] 3d^{9.36} 4s^{0.35} 4p^{0.64}, 5p^{0.02} in **1** and [Ar] 3d^{9.46} 4s^{0.26} 4p^{0.37}, 5p^{0.01} in **2**. Similarly, the natural atomic charges are Cu²⁺ = +0.638, Cl1 = -0.479, Cl2 = -0.622, N2 = -0.350, N3 = -0.287 and N4 = -0.507 in **1** and Cu²⁺ = +0.905, O1A = -1.015, O1B = -1.011, N1 = -0.557, N2 = -0.306 and N3 = -0.312 in **2**. For **1**, 17.996 electrons are distributed as core electrons, 10.341 electrons as valence on 4s, 3d and 4p orbitals and 0.025 electrons as Rydberg electrons on the 5p orbital, giving a total electron count of 28.362. This is compatible with the calculated natural charge of the Cu atom (+0.6382), which is correlated to the difference between 28.362 and the total number of electrons in an isolated copper atom (29 e). Likewise, the core, valence, Rydberg electrons and the natural charge on the copper atom in **2** are 17.994, 10.089, 0.012 and +0.905 respectively. Before complexation, the charge on a copper ion is +2, despite this fact, the charges on the copper(II) ions in complexes **1** and **2** are +0.638 and +0.905 respectively.

Second-order perturbation stabilization energies, analogous to the intermolecular charge transfer interaction (donor-acceptor), of the complexes were obtained using the B3LYP/LAN2DZ basis set. The computed intermolecular charge transfer energies (E) are 0.25 kcal/mol for **1** and 0.50

kcal/mol for **2**, due to the electron delocalization around the coordinated ligands. Complexes **1** and **2** may give rise to quite different intermolecular charge transfer energies. Complex **2** has a stronger (two times that of **1**) intermolecular charge transfer due to the presence of two bridged copper atoms. This is also confirmed from the results obtained for the frontier molecular orbitals' (HOMO and LUMO) energy gap (ΔE).

The HOMO-LUMO energy gap gives information about the reactivity and nature (soft or hard) of a molecule. The energies of six frontier molecular orbitals (FMOs) for complexes **1** and **2** had negative values, demonstrating that the present complexes are stable⁷¹. The energy gap (ΔE) values between E_{LUMO} and E_{HOMO} shows **1** > **2**. The ΔE value is also used to predict global reactivity descriptors, which additionally describe the internal charge transfer, susceptibility and stability of molecules⁷²⁻⁷⁵. Global reactivity descriptors, such as electronegativity (χ), global hardness (η), global electrophilicity (ω), electron donor capability (ω^-), electron acceptor capability (ω^+) and global softness (σ), were calculated using the formulas based on Koopman's theorem.

$$\text{Electronegativity } (\chi) = -\frac{1}{2} (E_{HOMO} + E_{LUMO})$$

$$\text{Global hardness } (\eta) = -\frac{1}{2} (E_{HOMO} - E_{LUMO})$$

$$\text{Global softness } (\sigma) = 1/\eta$$

$$\text{Electrophilicity } (\omega) = \chi^2 / 2\eta$$

$$\text{Electron donating capability } (\omega^-) = (3E_{HOMO} + E_{LUMO})^2 / 16(E_{HOMO} - E_{LUMO})$$

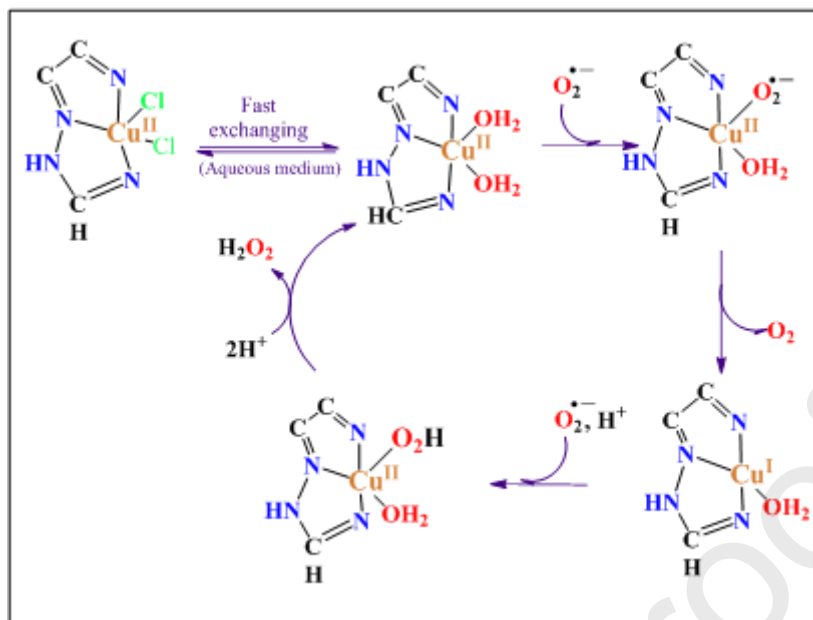
$$\text{Electron accepting capability } (\omega^+) = (E_{HOMO} + 3E_{LUMO})^2 / 16(E_{HOMO} - E_{LUMO})$$

The values of the global reactivity parameters are presented in Table S6. On perusal of these reactivity parameters, it was observed that all the parameters of **2** are greater than those of **1**, except the global hardness. This fact can be explained by complex **1** having a greater resistance to a change in the number of electrons. In complex **2**, the ligands could be more coordinated with the metal surface than in **1**⁷⁶. The dipole moment (μ) of these complexes is also estimated along different x , y and z coordinates. Table S7 displays the dipole moment value and its components along x , y and z directions. The results reveal that a higher value of μ is found for **1** compared to **2**. In the literature, the urea molecule is widely found as a reference for a comparison of dipole moments. The dipole moment of **1** is greater than that of the urea molecule, while that of **2** is less due to its symmetric structure⁷⁷.

3.11. Reactivity with superoxide

The superoxide anion ($O_2^{\cdot-}$) is often employed to obtain information on $M - O_2^{\cdot-}$ interactions. The *in vitro* antioxidant superoxide reactivity of the complexes has been evaluated using the alkaline DMSO-nitroblue tetrazolium (NBT) method⁷⁸⁻⁸⁰. The plot of the percentage inhibition (% Inhibition) is presented in Fig. 13. The concentrations for the reduction (IC_{50}) were determined for both complexes. The superoxide dismutase activity and catalytic constant (K_{cat}) were also evaluated. These SOD data are compared with similar known SOD mimics, as presented in Table 5^{78, 81-84}. The results reveal that both complexes are more efficient than Vitamin C (Vc), which is the standard for antioxidant superoxide dismutase^{15,53}. The SOD activity of complex **1** is higher than that of **2**. The SOD activities of present complexes are comparable to those of reported SOD mimics, but lower than the best-reported value. The difference in the SOD data between **1** and **2** may be ascribed due to the structural variation.

The catalytic SOD cycle based on the molecular structures is depicted in Scheme 5. The catalytic reaction starts when $O_2^{\cdot-}$ is electrostatically guided into the active site channel^{85,86}. It associates and binds directly to the copper(II) center and gives its electron via an inner-sphere mechanism. The oxygen molecule no longer charged and diffuses out of the active site channel. In the second half of the catalytic cycle, $O_2^{\cdot-}$ is electrostatically drawn into the active site channel. As the electron is accepted by the reduced copper center Cu(I) via an outer sphere electron-transfer mechanism, $O_2^{\cdot-}$ accepts a proton (H^+) simultaneously from the water molecule. The copper(II) ion can now move to reform the molecular structure and hydrogen peroxide (H_2O_2) diffuses out of the active site channel⁸⁷. This catalytic cycle permits the proposal of structure-based cyclic mechanism for Cu-Zn SOD catalytic action.



Scheme 5. The suggested mechanism of the O_2^- dismutation reaction catalyzed by a complex.

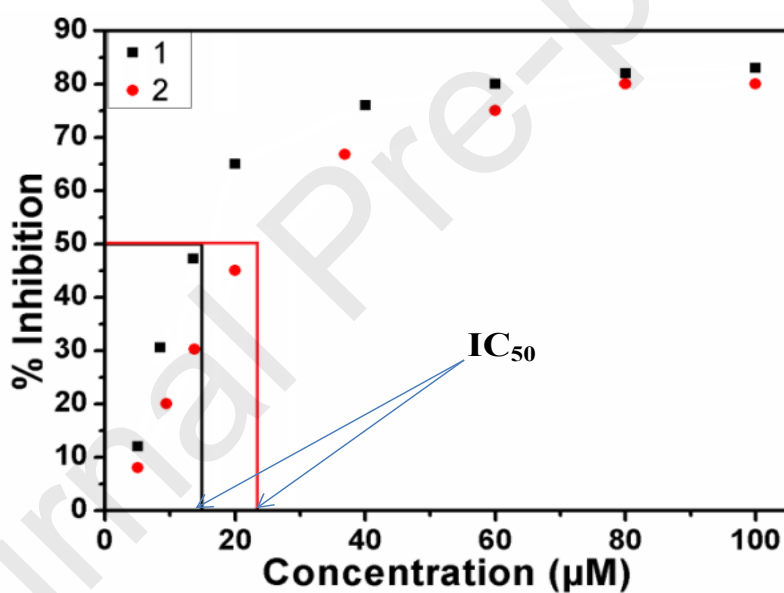


Fig. 13. A plot of % inhibition of NBT reduction vs concentration of complexes 1 and 2.

Table 5. SOD activities (IC_{50} values, kinetic catalytic constant and SOD activity) of Cu(II) complexes.

S. No.	Complex	IC_{50} (μM)	SOD activity (μM^{-1})	k_{cat} ($\text{M}^{-1}\text{s}^{-1}$)	Reference
1.	Vc	852	1.17	0.39	15,53
2.	$[\text{Cu}(\text{acetyl salicylate})_2]$	23	43.48	14.36	81,82
3.	$[\text{Cu}(\text{L})(\text{H}_2\text{O})]\text{NO}_3$	6	166.67	55.44	83,84
4.	$[\text{Cu}(\text{L})(\text{NO}_3)]$	16	62.50	20.79	83,84
5.	Native Cu-Zn SOD	-	0.04	25000	78
6.	$[\text{Cu}(\text{im})\text{Cu}(\text{pip})_2]_3^+$	0.50	2000	665.28	78
7.	$[\text{Cu}(\text{L})\text{Cl}_2]$	15	66.67	22.18	Present work
8.	$[\text{Cu}_2(\mu\text{-SO}_4)(\text{L})_2]$	22	45.45	15.12	Present work

L¹ = 4-chloro-2-((E)-[2-(pyridin-2-yl)hydrazinylidene]methyl}phenol.

3.12. Cytotoxicity assay

The anticancer activities of complexes **1** and **2**, and the ligand (**HL**) were assessed against four types of cancer cell lines, IMR 32 (neuroblastoma), MCF 7 (breast cancer), HepG2 (hepatocellular carcinoma) and A549 (lung cells), and the results were compared with the positive standard cisplatin under identical conditions using an MTT assay. The ability of a drug to inhibit cell proliferation is an important characteristic to prove its efficacy as a therapeutic drug. However, the major challenging aspect of synthesizing new chemotherapeutic agents is selectivity toward cancerous cells compared with normal cells⁸⁸⁻⁹⁰. It was found that the compounds in this study exhibit significant cytotoxic activities after 24 h of exposure. The IC₅₀ values (concentration required for 50% inhibition of cell growth) were calculated and the results are shown in Table 6. Cell growth was observed to be inhibited on increasing the concentration, indicating that **1**, **2**, **HL** and cisplatin have the potential to arrest cell survival. On comparing the different IC₅₀ values with that of cisplatin, all of **1**, **2** and **HL** show promising cytotoxicity on the selected cancerous cells in this study (A549, IMR322, HepG2 and A549). Among all the compounds, cell proliferation was depleted the most with exposure to **HL**. The IC₅₀ value for lung carcinoma cells on HL treatment was observed to be the lowest, whereas compounds **1** and **2** were more effective for hepatocellular carcinoma. Copper compounds are potentially cytotoxic because they exhibit a transition between Cu(II) and Cu(I) ions, which can result in the generation of superoxide and hydroxyl radicals, and thus induce cell death⁹¹. Hussain et al.⁹² suggested that Cu(II) complexes develop cytotoxicity in tumor cells; they recorded nuclear blebbing and fragmentation of nuclei on exposure to Cu complexes and highlighted them as apoptotic inducer in cancerous cells. From the preceding discussion, it is evident that both the complexes and the ligand showed better efficiency in terms of *in vitro* anticancer activity. In comparison to all cell lines, these compounds were observed to be more potent against HepG2 and A549 cell lines^{93,94}.

Table 6. The *in vitro* cytotoxic activity (expressed as IC₅₀ values) of the copper complexes against the different cell lines.

Compound	IC ₅₀ Value (μM)			
	MCF 7	IMR 32	HepG2	A549
1	105.6236	112.6543	101.209	119.194
2	184.2575	207.68	168.6424	174.107
Ligand	84.27725	87.56933	79.88781	75.169
Cisplatin	34.59	38.99	31.04	25.33

4. Conclusions

Two new mono and binuclear copper(II) complexes were synthesized by a biomimetic strategy and their structures were solved by single-crystal X-ray crystallography and various spectral techniques. All the copper centers in both complexes have pentacoordinate geometries. This kind of geometry has also been observed in some known di- or polynuclear copper(II) complexes^{95,96}. Low-temperature susceptibility measurements revealed that the copper(II) centers in both complexes **1** and **2** are weakly anti-ferromagnetically coupled. Complex **2** is a unique example showing ferro- and antiferromagnetic couplings. The ferromagnetic coupling in the two symmetric sulfate bridges fully agrees with previous magneto-structural correlations⁹⁷. The antioxidant SOD activities were also examined. Both complexes are potent SOD mimics. The structure-activity relationship for the complexes was studied to support the experimental findings and to assess some important parameters, *viz.* bond length, bond angle, HOMO-LUMO energy gap (ΔE), global reactivity descriptors, dipole moment, second-order perturbation energies and spin density. The antioxidant SOD and antiproliferative properties *in vitro* suggest the encouraging application of **1** and **2** in biology and pharmaceuticals sciences.

Acknowledgments

The authors are thankful to the Head, Department of Chemistry, MSU for providing the necessary facilities required to carry out this work. The authors are also thankful to SAIF IIT Mumbai for ESR measurements and SAIF CDRI Lucknow for microanalysis. M.C. and S.H. acknowledge the Spanish Ministerio de Economía y Competitividad (project CTQ2015-63858-P, MINECO/FEDER) and Comunidad de Madrid (project B2017/BMD-3770-CM) for providing financial support.

Funding

This research did not receive any specific grants from funding agencies in the public, commercial, or not-for-profit sectors.

Appendix A. Supplementary data

CCDC 1984430 and 1984431 contain the supplementary crystallographic data for complexes **1** and **2** respectively. These data can be obtained free of charge

via <http://www.ccdc.cam.ac.uk/conts/retrieving.html>, or from the Cambridge Crystallographic Data Centre, 12 Union Road, Cambridge CB2 1EZ, UK; fax: (+44) 1223-336-033; or e-mail: deposit@ccdc.cam.ac.uk.

References

1	B.P. Baranwal, K. Tripathi, A.K. Singh, S. Tripathi, <i>Spectrochim. Acta. A</i> 91 (2012) 365-369.
2	S. Ershad, L.-A. Sagathforoush, G.K. -Nezhad, S. Kangari, <i>Int. J Electrochem. Sci.</i> 4 (2009) 846-854.
3	B. Gao, M. Wan, J. Men, Y. Zhang, <i>Appl. Cataly. A Gen.</i> 439 (2012) 156-162.
4	M.H. Habibi, E. Shojaee, G.S. Nichol, <i>Spectrochim. Acta. A</i> 98 (2012) 396-404.
5	P. Bera, C.-H. Kim, S.I. Seok, <i>Solid State Sci.</i> 12 (2010) 532-535.
6	V. Madhu, S. Sabbani, R. Kishore, I.K. Naik, S.K. Das, <i>Cryst. Eng. Comm.</i> 17 (2015) 3219-3223.
7	I. Majumder, P. Chakraborty, S. Das, H. Kara, S.K. Chattopadhyay, E. Zangrando, D. Das, <i>RSC Adv.</i> 5 (2015) 51290-51301.
8	H. Tian, Z. Yu, A. Hagfeldt, L. Kloo, L. Sun, <i>J. Am. Chem. Soc.</i> 133 (2011) 9413-9422.
9	F. Arjmand, F. Sayeed, M. Muddassir, <i>J. Photochem. Photobiol. B Biol.</i> 103 (2011) 166-179.
10	L.P. Wu, T.K. Sowa, M. Maekawa, Y. Suenaga, M. Munakata, <i>J. Chem. Soc., Dalton Trans.</i> (1996) 2179-2180.
11	H. Zhang, D. Fu, F. Ji, G. Wang, K. Yu, T. Yao, <i>J. Chem. Soc., Dalton Trans.</i> (1996) 3799-3803.
12	P. A. Vigato, S. Tamburini, D. E. Fenton, <i>Coord. Chem. Rev.</i> 106 (1990) 25-170.
13	R. E. H. M. B. Os'orio, R. A. Peralta, A. J. Bortoluzzi, V. R. de Almeida, B. Szpoganicz, F. L. Fischer, H. Terenzi, A. S. Mangrich, K. Mary Mantovani, D. E. C. Ferreira, W. R. Rocha, W. Haase, Z. Tomkowicz, A. dos Anjos, A. Neves, <i>Inorg. Chem.</i> 51 (2012) 1569-2928.
14	M. Mugnai, G. Cardini, V. Schettino, C. J. Nielsen, <i>Mol. Phys.</i> 105 (2007) 2203-2210.
15	R.N. Patel, Y. Singh, Y.P. Singh, R.J. Butcher, A. Kamal, I.P. Tripathi, <i>Polyhedron</i> 117 (2016) 20-34.
16	S.K. Patel, R.N. Patel, Y. Singh, Y.P. Singh, D. Kumhar, R.N. Jadeja, H. Roy, A.K. Patel, N. Patel, N. Patel, A. Banerjee, D.C. -Lazarte, A. Gutierrez, <i>Polyhedron</i> 161 (2019) 198-212.
17	R.N. Patel, Y.P. Singh, Y. Singh, R.J. Butcher, M. Zeller, R.K.B. Singh, O. U-wang, <i>J. Mol. Struct.</i> 1136 (2017) 157-172.
18	R.N. Patel, Y.P. Singh, Y. Singh, R.J. Butcher, M. Zeller, <i>RSC Adv.</i> 6 (2016) 107379-107398.
19	R.N. Patel, Y.P. Singh, Y. Singh, R.J. Butcher, J.P. Jasinski, <i>Polyhedron</i> 133 (2017) 102-109.
20	R.N. Patel, Y.P. Singh, <i>J. Mol. Struct.</i> 1153 (2018) 162-169.
21	O. Pouralimardan, A.-C. Chamayou, C. Janiak, H.H. -Monfared, <i>Inorg. Chem. Acta.</i> 360 (2007) 1599-1608.
22	H. Ohtsu, Y. Shimazaki, A. Odani, O. Yamauchi, W. Mori, S. Itoh, S. Fukuzumi, <i>J.</i>

	Am. Chem. Soc. 122 (2000) 5733-5741.
23	A. Ray, C. Rizzoli, G. Pilet, C. Desplanches, E. Garribba, E. Rentschler, S. Mitra, Eur. J. Inorg. Chem. 2009 (2009) 2915-2928.
24	R.N. Patel, V.P. Sondhiya, K.K. Shukla, D.K. Patel, Y. Singh, Polyhedron 50 (2013) 139-145.
25	N.R. Sangeetha, K. Baradi, R. Gupta, C.K. Pal, V. Manivannan, S. Pal, Polyhedron 18 (1999) 1425-1429.
26	L.-M. Wu, H.-B. Teng, X.-C. Feng, X.-B. Ke, Q.-F. Zhu, J.-T. Su, W.-J. Xu, X.-M. Hu, Crys. Growth. Des. 7 (2007) 1337-1342.
27	M. Alagesan, N.S.P. Bhuvanesh, N. Dharmaraj, Eur. J. Med. Chem. 78 (2014) 281-293.
28	D.D. Perrin, W.L.F. Armango, D.R. Perrin, Purification of Laboratory Chemicals, Pergamon, Oxford, U.K., 1986.
29	G.M. Sheldrick, SHELXS-97, Program for the Solution of Crystal Structures, University of Göttingen, Göttingen, Germany, 1997.
30	G.M. Sheldrick, Acta Crystallogr. A46 (1990) 467.
31	G.M. Sheldrick, SHELXL-97, Program for the Refinement of Crystal Structures, University of Göttingen, Göttingen, Germany, 1997.
32	G.M. Sheldrick, Acta. Crystallogr. A64 (2008) 112-122.
33	G.A. Petersson, M.A. Al-Laham, J. Chem. Phys. 94 (1991) 6081-6090.
34	P.J. Hay, W.R. Wadt, J. Chem. Phys. 82 (1985) 270-283.
35	M.J. Frisch, G.W. Trucks, H.B. Schlegel, G.E. Scuseria, M.A. Robb, J.R. Cheeseman, G. Scalmani, V. Barone, B. Mennucci, G.A. Petersson, H. Nakatsuji, M. Caricato, X. Li, H.P. Hratchian, A.F. Izmaylov, J. Bloino, G. Zheng, J.L. Sonnenberg, M. Hada, M. Ehara, K. Toyota, R. Fukuda, J. Hasegawa, M. Ishida, T. Nakajima, Y. Honda, O. Kitao, H. Nakai, T. Vreven, J.A. Montgomery Jr., J.E. Peralta, F. Ogliaro, M. Bearpark, J.J. Heyd, E. Brothers, K.N. Kudin, V.N. Staroverov, R. Kobayashi, J. Normand, K. Raghavachari, A. Rendell, J.C. Burant, S.S. Iyengar, J. Tomasi, M. Cossi, N. Rega, J.M. Millam, M. Klene, J.E. Knox, J.B. Cross, V. Bakken, C. Adamo, J. Jaramillo, R. Gomperts, R.E. Stratmann, O. Yazyev, A.J. Austin, R. Cammi, C. Pomelli, J.W. Ochterski, R.L. Martin, K. Morokuma, V.G. Zakrzewski, G.A. Voth, P. Salvador, J.J. Dannenberg, S. Dapprich, A.D. Daniels, O. Farkas, J.B. Foresman, J.V. Ortiz, J. Cioslowski, D.J. Fox, Gaussian 09, Revision D.01, Gaussian Inc., Wallingford CT, (2009).
36	R. Bauernschmitt, R. Ahlrichs, Chem. Phys. Lett. 256 (1996) 454-464.
37	M. Cossi, N. Rega, G. Scalmani, V. Barone, J. Comput. Chem. 224 (2003) 669-681.
38	T. Mosmann, J. Immunol. 65 (1993) 55-63.
39	R.N. Patel, D.K. Patel, K.K. Shukla, Y. Singh, J. Coord. Chem. 66 (2013) 4131-4143.
40	R. G. Bhirud and T. S. Shrivastava, Inorg. Chim. Acta. 173 (1990) 121-125.
41	R. Konecny, J. Li, C.L. Fisher, V. Dillet, D. Bashford, L. Noodleman, Inorg. Chem. 38 (1999) 940-950.
42	M. Sutradhar, M.V. Kirillova, M.F.C.G. Silva, C.M. Liu, A.J.L. Pombeiro, Dalton Trans. 42 (2013) 16578-16587.
43	L. Valencia, R. Bastida, M.C.F. -Fernández, A. Macías, M. Vicente, Inorg. Chim. Acta. 358 (2005) 2618-2628.

44	A.W. Addison, T.N. Rao, J. Reedijk, J.V. Rijn, G.C. Verschoor, <i>J. Chem. Soc., Dalton Trans.</i> 7 (1984) 1349-1356.
45	N. Goel, U.P. Singh, <i>J. Phys. Chem. A</i> 117 (2013) 10428-11043.
46	N. Goel, N. Kumar, <i>J. Mol. Struct.</i> 1071 (2014) 60-70.
47	G.A. Jeffrey, W. Saenger, In: <i>Hydrogen Bonding in Biological Structures</i> , Springer-Verlag, Berlin, 1996, pp. 3-14.
48	O.P. Anderson, A.B. Packard, <i>Inorg. Chem.</i> 19 (1980) 2941-2945.
49	L.K. Thompson, S.K. Mandal, S.S. Tandon, J.N. Bridson, M.K. Park, <i>Inorg. Chem.</i> 35 (1996) 3117-3125.
50	J.K. McCusker, J.B. Vincent, E.A. Schmitt, M.L. Mino, K. Shin, D.A.K. Coggin, P.M. Hagen, J.C. Huffman, G. Christou, D.N. Hendrickson, <i>J. Am. Chem. Soc.</i> 113 (1991) 3012-3021.
51	M. Iqbal, I. Ahmad, S. Ali, N. Muhammad, S. Ahmed, <i>Polyhedron</i> 50 (2013) 524-531.
52	Y. Singh, R.N. Patel, S.K. Patel, A.K. Patel, N. Patel, R. Singh, R.J. Butcher, J.P. Jasinski, A. Gutierrez, <i>Polyhedron</i> 171 (2019) 155-171.
53	R.N. Patel, Y. Singh, Y.P. Singh, A.K. Patel, N. Patel, R. Singh, R.J. Butcher, J.P. Jasinski, E. Colacio, M.A. Palacios, <i>New J. Chem.</i> 42(2018) 3112-3136.
54	W.A. Alves, S.A. Almeida-Folho, R.H.A Santos, A.M.D.C. Ferreira, <i>Inorg. Chem. Commun.</i> 6 (2003) 294-299.
55	E. Garribba, G. Micera, <i>J. Chem. Educ.</i> 83 (2006) 1229-1232.
56	H. Guinaudeau, V. Elango, M. Shamma and V. Fajardo, <i>J. Chem. Soc., Chem. Commun.</i> (1982) 1122-1125.
57	H. Lavrenyuk, O. Mykhalichko, B. Zarychta, V. Olijnyk, B. Mykhalichko, <i>J. Coord. Chem.</i> 69 (2016) 2666-2676.
58	A. Bartyzel, <i>J. Therm. Anal. Calorim.</i> 131 (2018) 1221-1236.
59	S.Chandraleka, G.Chandramohan, <i>Afr. J. Pure Appl. Chem.</i> 8 (2014) 162-175.
60	(a) J.A. Bertrand, T.D. Black, P.G. Eller, F.T. Helm, R. Mahmood, <i>Inorg. Chem.</i> 15 (1976) 2965-2970; (b) H. Muhonen, <i>Inorg. Chem.</i> 25 (1986) 4692-4698; (c) N. Arulsamy, J. Glerup, D.J. Hodgson, <i>Inorg. Chem.</i> 33 (1994) 2066-2068; (d) W. Plass, A. Pohlmann, J. Rautengarten, <i>Angew. Chem.</i> 113 (2001) 4333-4333; (e) J. Tang, J.S. Costa, A. Golobi, B. Kozlev, A. Robertazzi, A.V. Vargiu, P. Gamez, J. Reedijk, <i>Inorg. Chem.</i> 48 (2009) 5473-5479; (f) A. Okazawa, T. Ishida, <i>Chem. Phys. Lett.</i> 480 (2009) 198-202; (g) M.S. Raya, A. Ghosh, R. Bhattacharya, G. Mukhopadhyay, M.G.B. Drew, J. Ribas, <i>Dalton Trans.</i> 252 (2004) 252-259; (h) C. Desplanches, E. Ruiz, S. Alvarez, <i>Chem. Commun.</i> (2002) 2614-2615; (i) C. Desplanches, E. Ruiz, A.R. -Fortea, S. Álvarez, <i>J. Am. Chem. Soc.</i> 124 (2002) 5197-5205; (j) F.A. Cotton, S. Herrero, R.J. -Aparicio, C.A. Murillo, F.A. Urbanos, D. Villagrán, X. Wang, <i>J. Am. Chem. Soc.</i> 129 (2007) 12666-12667; (k) M. Cortijo, R.G. -Prieto, S. Herrero, R.J. -Aparicio, P.S. -Rivera, <i>Eur. J. Inorg. Chem.</i> 32 (2013) 5523-5527; (l) M. Granelli, A.M. Downward, R. Huber, L. Guénée, C. Besnard, K.W. Krämer, S. Decurtins, S.-X. Liu, L.K. Thompson, A.F. Williams, <i>Eur. J. Chem.</i> 23 (2017) 7104-7112.
61	O. Khan, <i>Molecular Magnetism</i> , VCH Publishers: New York, 1993.
62	(a) S. Basak, S. Sen, P. Roy, C.G. -García, D.L. Huges, R.J. Butcher, E. Garriba, S. Mitra, <i>Aust. J. Chem.</i> 63 (2010) 479-489; (b) E. Ruiz, J. Cano, S. Álvarez, P. Alemany, <i>J. Am. Chem. Soc.</i> 120 (1998) 11122-11129; (c) V.H. Crawford, H.W.

	Richardson, J.R. Wasson, D.J. Hodgson, W.E. Hatfield, <i>Inorg. Chem.</i> , 15 (1976) 2107-2110.
63	K. Dankhoffa, B. Weber, <i>Cryst. Eng. Comm.</i> 20 (2018) 818-828.
64	A.D. Backe, <i>J. Chem. Phys.</i> 98 (1992) 5648-5692.
65	C. Lee, W. Yang, R.G. Parr, <i>Phy. Rev., B; Condens. Motor. Phys.</i> 37 (1988) 785-789.
66	Z. Zhou, R.G. Parr, <i>J. Am. Chem. Soc.</i> 112 (1990) 5720-5724.
67	J. Adhikary, P. Chakraborty, S. Das, T. Chattopadhyay, A. Bauza, S.K. Chattopadhyay, B. Ghosh, F.A. Mautner, A. Frontera, D. Das, <i>Inorg. Chem.</i> 52 (2013) 13442-13452.
68	A. Klien, D.A. Vicic, C. Biewer, I. Kietlch, K. Stirnat, C. Hamacher, <i>Organometallics.</i> 31 (2012) 5334-5341.
69	A.E. Reed, L.A. Curtiss, F. Weinhold, <i>Chem. Rev.</i> 88 (1988) 899-926.
70	S. Nawaz, A. Ghaffar, W. Zierkiewicz, M.M.-ul-Mehboob, Khurram, M.N. Tahir, A.A. Isab, S. Ahmad, <i>J. Mol. Struct.</i> 1137 (2017) 784-791.
71	R. Jawari, M. Hussian, M. Khalid, M.U. Khan, M.N. Tahir, M.M. Naseer, A.A.C. Braga, Z. Shafiq, <i>Inorg. Chim. Acta.</i> 486 (2019) 162-171.
72	R.G. Parr, L. Szentpály, S. Liu, <i>J. Am. Chem. Soc.</i> 121 (1999) 1922-1924.
73	R.G. Parr, R.A. Donnelly, M. Levy, W.E. Palke, <i>J. Chem. Phys.</i> 68 (1978) 3801-3807.
74	P.K. Chattaraj, U. Sarkar, D.R. Roy, <i>Chem. Rev.</i> 106 (2006) 2065-2091.
75	A. Lesar, I. Milošev, <i>Phys. Lett.</i> 483 (2009) 198-203.
76	A. Kokalj, <i>Chem. Phys.</i> 393 (2012) 1-12.
77	P.N. Prasad, D.J. Williams, <i>Introduction to non-linear effect in molecules and polymer</i> , John Wiley & Sons, New York, 1991.
78	U. Weser, L.M. Schubotz, E. Lengfelder, <i>E. J. Mol. Catal.</i> 13 (1981) 249.
79	Y.P. Singh, R.N. Patel, Y. Singh, D.C. –Lazarteb, R.J. Butcher, <i>Dalton Trans.</i> 46 (2017) 2803-2820.
80	R. Konecny, J. Li, C.L. Fisher, V. Dillet, D. Bashford, L. Noodleman, <i>Inorg. Chem.</i> 38 (1999) 940-950.
81	B.J. Hathaway, <i>Structure and Bonding</i> , Berlin, 57 (1984) 55-118.
82	E. Garriba, J. Micera, <i>J. Chem. Educ.</i> 83 (2006) 1229-1232.
83	A.K. Patel, R.N. Jadeja, H. Roy, R.N. Patel, S.K. Patel, R.J. Butcher, <i>J. Mol. Struct.</i> 1185 (2019) 341-350.
84	Y. Singh, R.N. Patel, Y.P. Singh, A.K. Patel, N. Patel, R. Singh, R.J. Butcher, J.P. Jasinski, E. Colacio, M.A. Palacios, <i>Dalton Trans.</i> 46 (2017) 11860-11874.
85	R.G. Bhirud, T.S. Srivastava, <i>Inorg. Chim. Acta</i> 173 (1990) 121-125.
86	E.D. Getzoff, J.A. Tainer, M.M. Stempien, G.I. Bell, R.A. Hallewell, <i>Proteins</i> 5 (1989) 322-336.
87	E.D. Getzoff, D.E. Cabelli, C.L. Fisher, H.E. Parge, M.S. Viezzoli, L. Banci, R.A. Hallewell, <i>Nature</i> 358 (1992) 347-351.
88	J. Qi, Y. Gou, Y. Zhang, K. Yang, S. Chen, L. Liu, X. Wu, T. Wang, W. Zhang, F. Yang, <i>J. Med. Chem.</i> 59 (2016) 7497-7511.
89	M.C. Alley, D.A. Scudiero, A. Monks, M.L. Hursey, M.J. Czerwinski, D.L. Fine, B.J. Abbott, J.G. Mayo, R.H. Shoemaker, M.R. Boyd, <i>Cancer Res.</i> 48 (1988) 589.
90	S.S. Bhat, A.A. Kumbhar, H. Heptullah, A.A. Khan, V.V. Gobre, S.P. Gejji, V.G. Puranik, <i>Inorg. Chem.</i> 50 (2011) 545.

91	B. Paul, T. Chounwou, C. Newsome, J. Williams, K. Glass. <i>Met. Ions Biol. Med.</i> 10(2008) 285-290.
92	A. Hussain, M.F. AlAjmi, M.T. Rehman, S. Amir, F.M. Husain, A. Alsalmeh, M. A. Siddiqui, A.A. Alkhedhairi, R.A. Khan, <i>Sci. Rep.</i> 9(2019)5237.
93	F.R.G. Bergamini, J.H.B. Nunes, M.A. de Carvalho, M.A. Ribeiro, P.P. Pavia, T.P. Banzato, A.L.T.G. Ruiz, J.E. Carvalho, W.R. Lustri, D.O.T.A. Martins, A.M.C. Ferreria, P.P. Corbi, <i>Inorg. Chim. Acta.</i> 484 (2019) 491-502.
94	J. Wang, Y. Gou, Z. Zhang, P. Yu, J. Qi, Q. Qin, H. Sun, X. Wu, H. Liang, F. Yang, <i>Mol. Pharmaceutics.</i> DOI:10.1021/acs.molpharmaceut.8b00045.
95	G.A. van Albada, J.G. Haasnoot, J. Reedijk, M. Cingi-Biagini, A.M. Manotti-Lanfredi, F. Ugozzoli, <i>Polyhedron</i> 14 (1995) 2467-2473.
96	J.E. Bol, W.L. Driessen, J. Reedijk, <i>J. Chem. Soc., Chem. Commun.</i> (1995) 1365.
97	S. Naiya, C. Biswas, M.G.B. Drew, C.J. Gomez-Garcia, J.M. Clemente-Juan, A. Ghosh, <i>Inorg. Chem.</i> 49 (2010) 6616-6627.

Credit authorship contribution statement

Abhay kumar Patel: Funding acquisition, Investigation, Methodology.

R. N. Jadeja: Conceptualization, Supervision, Visualization, Writing - original draft, Writing - review & editing.

R. N. Patel: Conceptualization, Project administration, Resources, Software, Visualization, Writing – original draft.

S. K. Patel: Project administration, Resources, Software.

Hetal Roy: Formal analysis.

M. Cortijo and S. Herrero: Data creation, Validation.

R. J. Butcher: Data creation, Validation.

Declaration of interests

The authors declare that they have no known competing financial interests or personal relationships that could have appeared to influence the work reported in this paper.

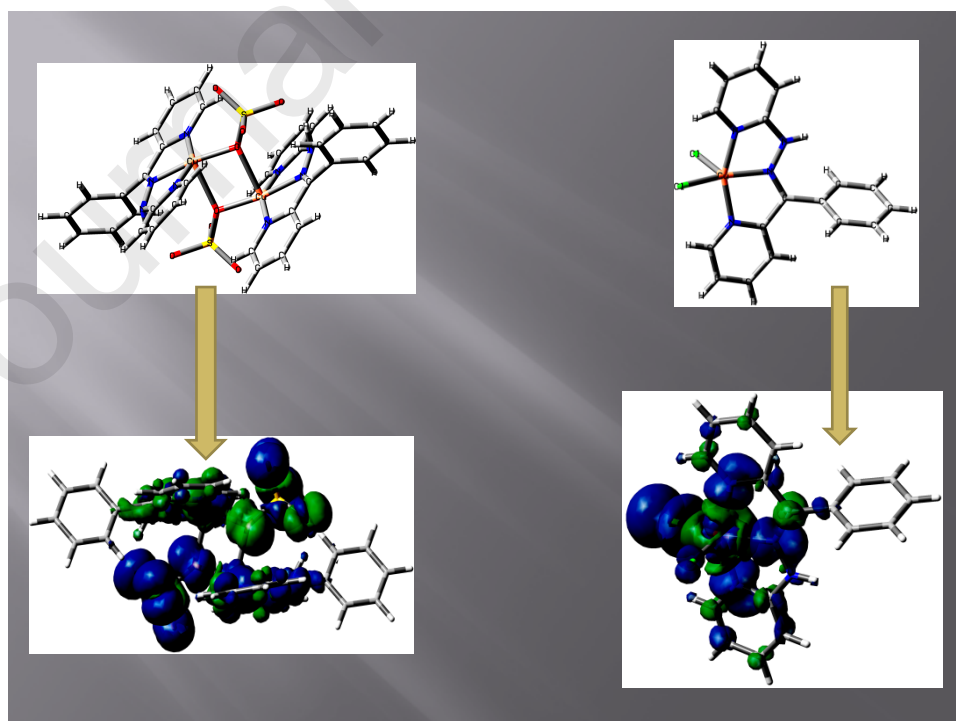
The authors declare the following financial interests/personal relationships which may be considered as potential competing interests:

'Declarations of interest: none'

Highlights

- Synthesis and characterization of two copper(II) hydrazone complexes.
- The copper complexes are mono and binuclear, having distorted square pyramidal geometries.
- Both complexes show a weak anti-ferromagnetic interaction.
- Both complexes catalyzed the dismutation of superoxide (O_2^-).
- Both complexes show good cytotoxicity against cancers cell lines.

Graphical Abstract (Pictogram)



Graphical abstract (Synopsis)

Two new mono and binuclear copper(II) complexes were synthesized by a biomimetic strategy and their structures were solved by single-crystal X-ray crystallography and various spectral techniques. Both complexes have pentacoordinate geometries. Low-temperature susceptibility measurements revealed that the copper(II) centers in both complexes are weakly antiferromagnetically coupled. Their antioxidant SOD and anticancer activities were also examined. Both complexes are potent SOD mimics and display anticancer activity.